PROJECT SQUID

TECHNICAL REPORT CIT-7-PU

LARGE STRUCTURE DYNAMICS AND ENTRAINMENT IN THE MIXING LAYER AT HIGH REYNOLDS NUMBER

BY

PAUL E. DIMOTAKIS
AND
GARRY L. BROWN
GRADUATE AERONAUTICAL LABORATORIES
CALIFORNIA INSTITUTE OF TECHNOLOGY
PASADENA, CALIFORNIA

PROJECT SQUID HEADQUARTERS
THERMAL SCIENCE AND PROPULSION CENTER
PURDUE UNIVERSITY
WEST LAFAYETTE, INDIANA

AUGUST 1975

Project SQUID is a cooperative program of basic research relating to Jet Propulsion. It is sponsored by the Office of Naval Research and is administered by Purdue University through Contract N00014-75-C-1143, NR-098-038.

Project SQUID Technical Report CIT-7-PU

LARGE STRUCTURE DYNAMICS AND ENTRAINMENT IN THE MIXING LAYER AT HIGH REYNOLDS NUMBER.

by

Paul E. Dimotakis

and

Garry L. Brown[†]

Work performed under Contract No. 4965-42 for Project SQUID and Contract No. N00014-67-A-0094-0037 for the Fluid Dynamics Program of the Office of Naval Research

Graduate Aeronautical Laboratories

California Institute of Technology

Pasadena, California

August, 1975

[†]On study leave from the University of Adelaide.

ABSTRACT

Observations were made on a turbulent mixing layer in a water channel at Reynolds numbers up to 3×10^6. Flow visualization with dyes revealed (once more) large coherent structures and showed their role in the entrainment process; observations of the reaction of a base and an acid indicator injected on the two sides of the layer, respectively, gave some indication of where molecular mixing occurs. Autocorrelations of streamwise velocity fluctuations, using an LDV, revealed a fundamental periodicity associated with the large structures. The surprisingly long correlation times suggest time scales much longer than had been supposed; it is argued that the mixing layer dynamics at any point is coupled to the large structure further downstream, and some possible consequences about the effects of initial conditions and of the influence of apparatus geometry are discussed.

I. Introduction

It is becoming increasingly evident that the classical picture of turbulence, as a state of flow in which the properties of the various dynamic variables can only be determined in a stochastic sense, is not quite complete. Experimental results in the last few years indicate that within the obvious randomness of turbulence there exist flow patterns and large scale structures that appear dominant in determining the overall characteristics of such flows. A notable example can be found in the discovery that the turbulent mixing layer is inhabited by a more or less organized large structure (Brown and Roshko 1971).

Large scale vortices and instabilities at very high Reynolds number had been found in other flows. Yet the apparent quasi-regularity that is manifest in the photographs and high speed motion pictures of Brown and Roshko (1971 and 1974) was not expected. It was unexpected because such well-defined structure is far from random and appears inconsistent with the classical picture of turbulence. Even though such apparent inconsistencies are probably adequately explained, in terms of the irregularity and jitter in the formation, amalgamation, and spacing of these large structures (Brown and Roshko 1974), important questions remain to be answered. It becomes important, for example, to establish whether these large structures persist at even higher Reynolds numbers or whether they are a curious transition from the well-defined periodicity of the laminar instability region (Sato 1956), to a state of complete randomness at infinite Reynolds number. In addition, the question of persistence of the mechanism of vortex pairing, well documented at relatively low

Reynolds number (Winant and Browand 1974), arises, especially since this mechanism is not so apparent in the photographs and motion pictures of Brown and Roshko taken at much higher Reynolds numbers.

With these questions in mind, the experiment described here was undertaken. It was decided to take advantage of the GALCIT 50 cm x 50 cm Free Surface Water Tunnel, which has a 2.4 meter (8 foot) long test section and is capable of reaching a test section velocity of 7.6 m/sec. To generate the shear layer, an insert was designed for the test section yielding a velocity ratio between the two streams of 5:1.

Water offers several attractive features as the flowing medium. The most important of these, for our purposes, was the high Reynolds number per unit length and velocity. In addition, and as a consequence of the relatively low velocities required, flow visualization by dye injection is particularly simple. Lastly, it was possible to take advantage of high accuracy and high spatial and temporal resolution of a newly developed single-particle laser Doppler velocimeter, water being an ideal medium for this measurement technique.

By injecting dye for flow visualization, we were able to observe and photograph the large structure and follow the process of entrainment by direct observation and motion pictures. Replacing the dye by an acid containing a pH indicator on one side and by a base on the other side of the layer, we obtained photographs as well as a motion picture in which the chemical reaction between the two, as they were entrained and mixed in the layer, was qualitatively marked by the change in color of the indicator.

The flow visualization evidence for the existence of the large structure at a high Reynolds number (3×10^6) is unmistakable and its dominant role in the entrainment process is manifest.

The autocorrelation function of the streamwise velocity fluctuations revealed a fundamental periodicity which was found to be consistent with the expected similarity scaling. Other features of the data, however, cannot be explained quite so simply and it now appears that similarity in the broad sense does not account for much of the observed behavior. More complicated processes seem to govern the dynamics of the flow than can be explained in terms of local phenomena. Mechanisms for coupling the whole shear layer are required and suggest that such factors as initial conditions are always important. These preliminary experiments perhaps raise more questions than they can answer. Nevertheless, we feel that the results presented here are of sufficient interest in themselves and important in that they do raise these questions.

2. Apparatus and Resulting Flow Field

The high Reynolds numbers which may be achieved in the 50 cm x 50 cm GALCIT Free Surface Water Tunnel made this facility a logical choice for the experiment. This tunnel is capable of a maximum velocity, without a model in the 2.4 meter working section, of 7.6 m/sec. It was decided to modify this facility in such a way as to generate a well defined, two-dimensional shear layer with a high aspect ratio. Unfortunately, to obtain a shear layer, with a large velocity ratio, in two separate streams within the test section of a conventional wind or water tunnel is by no means straightforward. This is especially true if it is not feasible to divide the flow into two parts, within the tunnel contraction. In several other attempts to establish two streams of different velocity in a tunnel test section by dividing the flow and placing flow resistance on the low speed side, there appear to have been difficulties with flow separation and flow nonuniformity as the velocity ratio becomes large. Having a velocity of zero on the low speed side may appear to avoid these problems but, in the GALCIT Water Tunnel at least, to satisfy the entrainment requirements while maintaining a low-turbulence high-quality flow would render this choice an even more difficult problem. Consequently, we decided to design an insert that would produce a shear layer with a non-zero U_2 within the water tunnel test section, taking special precautions to minimize the possibility of separation. The outcome is shown in figure 1 and the manner in which it is placed in the working section is shown in figure 2. The resulting apparatus proved to be very satisfactory and the basis for the design of the insert possibly merits a brief description. In order to avoid separation at the leading edge of the flow divider, it is desirable to design

the two flow paths to have exactly the same pressure drop for a given inlet velocity. For an area contraction ratio of $A_{in}/A_{out} = C_A$, on the high speed side, and a corresponding expansion of $1/C_A$ on the low speed side, matched inlet and exit pressures and uniform flow at the two inlets ensures that the velocity ratio $r \equiv U_1/U_2$ is equal to C_A^2. The flow resistance on the low speed side must match the Bernoulli pressure drop in the high speed side. The flow must also be redirected within the expansion to avoid separation. The two perforated plates shown in figure 1 (50% open) were correspondingly located at places where separation might otherwise have occurred. The plates were curved (rolled as segments of a circle) to be approximately perpendicular to the stream-lines of an inviscid flow through the expansion. Adjustment was provided by allowing movement of the lower edge of the plate upstream and the upper edge downstream or vice versa so that the flow could be directed more toward the lower or upper boundary. Fine control and adjustment of the pressure drop was obtained by placing an identical perforated sheet on top of the first. Sliding one vertically relative to the other resulted in a variable percentage open area. This, of course, had some effect on the flow direction after the plate, which had to be offset, as required, by tilting the plate. Finally, the resulting turbulence on the low speed side was reduced in scale and amplitude and the flow made even more uniform by the 40 mesh, 50% open screen placed at the exit of the expansion. The percentage open area (solidity) of the plates and the screen as well as their location were chosen to provide the requisite total pressure coefficient. Handbook data were used to compute the individual pressure drops. Perforated plates were chosen to provide the flow

resistance because the pressure drop across them is very nearly Reynolds number independent and because they have sufficient thickness to provide in-plane forces that tend to give an exit flow velocity that is perpendicular to the surface of the plate (hence the curved shape). In addition to this insert, a 150 cm long lucite top was installed in the remainder of the test section to remove free surface effects of various kinds (see Fig. 2).

Just downstream of the insert, the flow on the low velocity side was found to be uniform within 1% of the high velocity stream over the full 35 cm flow width. The measured velocity ratio, $r = U_2/U_1$, was 0.21 at a U_1 of 165 cm/sec. At the first measuring station, 15 cm downstream from the end of the splitter plate, the root mean square fluctuation of the velocity measurements in the free stream on the high speed side was less than 0.5% of U_1 (no attempt was made to distinguish low frequency velocity fluctuations, turbulence and electronic noise - this is then an upper bound for the turbulence level). On the low speed side it was less than 2% of U_2, which, since U_2 is much less than U_1, is also very small compared with the relevant velocity $U_1 - U_2$. In general, the whole flow was very steady (less than 1% long term variation in free stream velocity) over many hours of operation, except for some small low frequency fluctuations in free stream velocity, observed at the measuring station farthest downstream, probably due to surface waves downstream of the 150 cm lucite top.

At a free stream velocity on the high speed side of 165 cm/sec, the boundary layer momentum thickness was of the order of 0.4 mm, while the maximum slope thickness, 12 mm downstream of the splitter plate trailing edge, was 2 mm. The mean velocity profiles, at a high

speed free stream velocity of 165 cm/sec where most of the data were taken, are plotted in similarity coordinates in figure 3. They represent measurements at 15 cm, 30 cm, 60 cm and 90 cm downstream of the splitter plate. Each point is the time-averaged velocity computed from several records of 1,024 discrete measurements, in a manner described in section 4. No quantitative velocity data were recorded any further downstream in order to restrict the data to an aspect ratio for the large structure (span to vorticity thickness ratio) as large as possible. From the flow visualization data, however, it was clear that, at least qualitatively, the same basic two-dimensional large structure persisted to the end of the working section, i.e., for an additional distance about twice that of the farthest measuring station. See figure 4 (plate 1).

We were surprised to find the scatter in the mean profile data as large as it was. For those points, particularly near the dividing streamline, where several records of 1,024 measurements were taken, variations of as much as 5 to 10% were found between estimates of the mean velocity obtained from each record. It now seems likely that the averaging intervals, during which the 1,024 velocity samples were recorded, may not have been long enough. This becomes a more definite possibility in view of the surprisingly long time scales that were found to characterize the flow dynamics.

The mean velocity profile does not seem to have attained the self-similar shape by x = 15 cm. The vorticity (maximum slope) thickness, for stations farther downstream, was estimated to be

$$0.10 \leqslant \frac{\delta_\omega}{x - x_o} \leqslant 0.13 \qquad (1)$$

This is consistent with the range of values of the data collected by Brown and Roshko (1974) in their figure 10, corresponding to

$$\lambda \equiv \frac{U_1 - U_2}{U_1 + U_2} \simeq 0.65 \quad , \tag{2}$$

and very close to the result at a comparable velocity ratio obtained by Spencer and Jones (1971).

3. Flow Visualization Results

As mentioned previously, a particular advantage of conducting such an experiment in a water tunnel is the simplicity of flow visualization using dye injection. Also, the relatively low velocities required and the large available dimensions of the facility make for simple photographic techniques.

It would probably have been advantageous to flood the whole low speed side with dye so as to label one stream completely. The required amount of dye, however, would have contaminated the closed tunnel circuit very quickly. Consequently it was decided to inject dye locally from the base of two two-dimensional airfoil sections spanning the tunnel test section at zero angle of attack. Commercially available airfoil-shaped tubing (12mm chord, 3mm thickness) was used with thin slots milled in the base over the central 1/3 of the span. Ideally it should be possible to inject the dye at the base at the local fluid velocity so that in uniform flow it is confined to the thin wake of the airfoil. This ideal was not approximated as well as it might have been as the trailing edge of the airfoil tubing was relatively thick (1.5mm) and the dye was essentially injected in separated flow. By changing the position of the airfoil injectors it was possible to ascertain that they had no discernible effect on the large scale structure being observed.

The flow visualization was carried out with a free stream velocity on the high speed side of 100 cm/sec, without the lucite top to permit the injectors to be installed. This velocity was chosen because the corresponding low speed side velocity was subcritical (< 23 cm/sec) with respect to surface waves, resulting in a quiescent free surface. To investigate the entraining process and to see the large structure

more clearly, the two dye injectors were placed just above and just below the edge of the mixing layer at a distance 30 cm downstream of the splitter plate. Photographs obtained by alternately injecting from the high speed side and the low speed side are shown in figures 4a and 4b (plate 1), respectively (flow is from right to left, high speed side is on the bottom).

It appears that the entrainment of fluid into the layer is a more or less symmetric mechanism (in a frame of reference moving with the convection velocity of the large structure, to be more exact). One can also conclude that the initial stages of this mechanism appear more a process of engulfment in which the velocity induced in the two free streams by the large structure (approximately a two-dimensional vortex) causes the freshly entrained fluid in the neighborhood of this structure to penetrate well into the layer. Dye, labeling fluid from one side, can be seen to cross all the way into the other side before any small scale mixing occurs. This is perhaps more clearly seen in figure 5 (plate 2) in which dyes of different colors have been injected from each side at the same time. Note the similarity between this picture and the photographs of Brown and Roshko (1974).

Once inside the layer, the freshly entrained fluid appears associated with the irrotational part of the large scale motion of the nearest large structure and remains distinguishable during that large structure's lifetime. It seems to mix, however, very rapidly and down to very small scales throughout the layer once the identity of the particular large structure is lost by some means or other. This latter behavior was more clearly seen in the movies and by direct observation.

To investigate this final stage of the mixing process more directly and to obtain a qualitative feeling for the rapidity of the subsequent molecular mixing, a different scheme was employed. The

blue dye was replaced with a solution of nitric acid containing bromothymol blue, a pH indicator, and the red dye was replaced by a (colorless) ammonium hydroxide solution. The bromothymol blue changes from a deep orange, in an acid environment to deep blue in the alkali, the change occurring close to a pH of 7. A photograph of this change occurring in the mixing layer, as the entrained acid solution reacted with the entrained alkaline solution, is shown in figure 6 (plate 2). Note, from figures 4a, 4b and 5, that the center of the shear layer is approximately located halfway between the two bottom dots on the right hand side of the picture (threaded inserts in the tunnel lucite sidewalls). The acid in the picture (orange) has already entered the shear layer (δ_{viz} of Brown and Roshko 1974) and can be seen to participate in the large structure motion. It does not react (blue), however, until a later time. It can be seen that, at these Reynolds numbers, the reaction, once it begins, occurs almost instantaneously indicating the high efficiency of small scale mixing in the latter stages of entrainment, and consistent with the observations with the inert dyes described above. If the decrease in the characteristic scales of the entrained fluid occurred by means of a gradual process, regions of unreacted fluid would have been discernible for a greater distance. The length scale of this gradual process would have been of the order of the large structure size. This is not the case as can be seen in figure 6. The Reynolds number, based on the velocity of the high speed side and the distance from the center of the photographic plates to the splitter plate trailing edge, was equal to 2×10^6.

Thus, it would appear that the processes of entrainment and fine scale mixing, at high Reynolds numbers, are almost distinct and separate stages. This observation is also in agreement with some new detailed measurements, in the Brown and Roshko (1974) gas mixing apparatus, obtained by Brown and Konrad (to be published). It is also interesting to note that the details of the initial stages of the entrainment process, described above, are almost identical to the observations of Winant and Browand (1974), at much lower Reynolds numbers.

With the aid of the flow visualization it was also possible to observe the interaction between the large structure at these Reynolds numbers. The mechanism of pairing (or tripling), observed by Winant and Browand (1974) at much lower Reynolds numbers, does not appear to be the predominant means by which the large scale structures amalgamate and maintain a separation which on the average is proportional to the value of the downstream coordinate. While pairing is occasionally observed, a more violent process seems to be mainly responsible for the disappearance of identifiable structures, in their procession down the shear layer. This process is better seen in the motion pictures and by direct observation and is perhaps better described as "tearing." It appears that one or occasionally more structures find themselves in the vicinity of two neighboring others, in whose straining field they disintegrate. The fluid associated with the structure that "disappears" becomes part of the collective motion of the neighboring structures as they compete for different parts of it. This picture is very similar, in many respects, to the one proposed by Moore and Saffman (1974).

In this general context, the dominant role of the dynamics and interaction of the large structure, in the overall mechanism that eventually brings the two fluids in intimate contact, becomes apparent. It is clear that any theoretical attempts to model the complex mixing process in the shear layer must take this ubiquitous large structure into account.

4. Velocity Measurement Instrumentation and Data Processing.

The streamwise velocities were measured using a single-particle laser Doppler velocimeter (Dimotakis and Lang 1974) in the reference-scatter mode. See figure 7. The apertures at the receiving end were chosen to include the full beam width of the reference beam. Thus the scattering angle θ was defined as the angle subtended by the scattering beam axis and the reference beam axis, the reference beam serving as the spatial filter (Siegman 1966, Mayo 1970). It was measured to be $\theta = 4.694°$, resulting in a fringe spacing in the overlap volume of (Helium-Neon laser, $\lambda = 0.6328$ μm)

$$\frac{\lambda}{2 \sin \frac{\theta}{2}} = 7.725 \text{ μm},$$

and a Doppler constant of

$$\frac{2}{\lambda} \sin \frac{\theta}{2} = 1.295 \left(\frac{\text{kHz}}{\text{cm/sec.}} \right).$$

The actual velocity measurement consisted of measuring the time of flight of a single scattering particle for a distance corresponding to eleven fringe planes (ten intervals). The real time of each event was recorded by reading a free-running counter, counting a crystal controlled time base. The average data rate was monitored and could be controlled by adjusting the level that the amplitude of the signal burst, due to a single particle, had to cross to be processed. As the level was raised, fewer particles could meet this criterion and the data rate decreased (Dimotakis 1976). The limitation on the velocity measurement accuracy appeared to be connected with

nonuniformity of the fringe plane spacings in the focal volume. This was due to optical aberrations introduced by the 10cm thick lucite water tunnel windows, through which the measurement had to be made. In the absence of such aberrations, it can be shown that no ambiguity exists between the measured time of flight of a single scattering particle, for a distance corresponding to a fixed number of fringe planes, and the velocity component of the particle perpendicular to the fringe planes. A more detailed discussion of this point, along with other general considerations related to this method of measurement, are examined separately (Dimotakis 1975).

The time of flight and real time for each particle are coded into a single 32-bit word and stored in a 2 x (1024 x 32) high speed buffer memory and subsequently recorded on a Kennedy 1600/360 incremental tape recorder, operated in the slewing mode. A block diagram of the signal processing and data acquisition appears on figure 8.

The resulting tape is processed, record by record, to yield the data

$$\{(t_i,\ u_i),\ i = 1, N\}\ ,$$

where t_i is the real time of the i^{th} particle crossing, u_i its streamwise velocity component and N = 1,024. Sample data are presented in figures 9a, 9b, and 10. Each figure represents one data record consisting of 1,024 individual measurements as described above.

In computing the various stochastic quantities of interest from such data, care should be exercised in the choice of algorithms

in view of the inherent sampling bias of this method of measurement (McLaughlin and Tiederman 1973, Barnett and Bentley 1974, Dimotakis 1976). In particular, algorithms approximating time integrals, as opposed to (unweighted) ensemble averages should be preferred. For example, mean velocities are best computed as

$$\bar{u} = \frac{1}{T} \sum_{i=2}^{N} u_i \, \delta t_i \tag{3a}$$

where

$$T = t_N - t_1 \tag{3b}$$

and

$$\delta t_i = t_i - t_{i-1} \, . \tag{3c}$$

This estimate can differ by a few percent, depending on the sampling process details and the velocity distribution function, from the biased ensemble average,

$$\langle u \rangle_b = \frac{1}{N} \sum_{i=1}^{N} u_i \tag{4}$$

(Dimotakis 1976).

The errors can be more serious in computing the autocorrelation function, where errors resulting from subtracting the incorrect mean can be misinterpreted as correlations for large time shifts. The autocorrelations presented in the subsequent sections were computed in the following manner. Any small parabolic trend was removed from each record, i.e.,

$$u_i' = u_i - \bar{u} - (b_o + b_1 t_i + b_2 t_i^2) \qquad (5)$$

where $\bar{u}$ was computed in terms of Eq. 1 and b_o, b_1, b_2 were chosen to satisfy the condition

$$\sum_{i=2}^{N} \left[u_i - \bar{u} - (b_o + b_1 t_i + b_2 t_i^2)\right]^2 \delta t_i = \text{min.}$$

The autocorrelation function was then computed by the algorithm

$$R_{uu}(\tau) = \frac{1}{t_M - t_1} \sum_{i=2}^{M} u_i' \, u'(t_i+\tau) \, \delta t_i, \qquad (6a)$$

where M is the largest index such that $t_M + \tau < t_N$ and $u'(t_i + \tau)$ is the linearly interpolated value of the velocity at $t = t_i + \tau$, i.e.,

$$u'(t_i+\tau) = u_{j-1}' + (t_i + \tau - t_{j-1}) \, \delta u_j'/\delta t_j, \qquad (6b)$$

where

$$t_{j-1} < t_i + \tau < t_j$$

$$\delta t_j = t_j - t_{j-1}$$

and

$$\delta u_j' = u_j' - u_{u-1}' \, . \qquad (6c)$$

The autocorrelation function was never computed for shifts τ corresponding to less than the mean sampling interval

$$\tau_s = \frac{T}{N-1} \, . \qquad (7)$$

In addition, only records containing more than four large structures but less than thirty were used. The upper limit of thirty was imposed

because of the finite number of points per record (1,024). Within these two limits there were enough structures in the record for the fundamental frequency to be determinable and enough measurements per large structure cycle to justify the numerical time-integration scheme.

A free stream velocity of U_1 = 330 cm/sec was the highest velocity at which quantitative measurements were recorded. Efforts to record data at higher velocities were frustrated by an unexpected difficulty. Small particles, rust, mud and general debris were picked up from other parts of the circuit by the higher speed flow, seriously impairing visibility in the test section and rendering the laser Doppler velocity measurements difficult. An improved filtration system, that has since been installed, will permit measurements at the higher velocities that can be attained in this facility (an increase greater than a factor of two in the Reynolds number).

5. Velocity Measurements and Autocorrelation Functions

Most of the velocity measurements were made just outside the shear layer, corresponding to a similarity coordinate of

$$\eta - \eta^* = \frac{y - y^*}{x - x_o} \sim \pm \frac{1}{8} \quad .$$

x_o and y_o are the coordinates of the virtual origin of the shear layer and

$$\eta^* = \frac{y^* - y_o}{x - x_o}$$

is the similarity coordinate of the ray on which the mean velocity is given by

$$U(\eta^*) = \frac{1}{2}(U_1 + U_2) \quad . \tag{8}$$

As can be seen from figure 3 of the velocity profiles, these measurement locations correspond to a local mean velocity that is almost equal to that of the corresponding free stream (U_1 or U_2). One might conclude from this observation that the amplitude of the local fluctuations in the streamwise velocity would be small. The sample data, however, presented in figures 9a, 9b and 10 show quite the contrary. Several observations and conclusions can be made from these data samples.

One would be forced to deduce, from such data alone, the existence of a large organized structure within the shear layer. These fluctuations, measured in the neighboring free stream, could not have been caused by small, randomly distributed and randomly oriented domains of high turbulence activity within the shear layer. The effect from many such small domains would have been essentially cancelled by the superposition of the various uncorrelated disturbances and

attenuated by the distance between the measurement location and the corresponding region in the shear layer, as scaled by the characteristic size of these domains. In fact, the effect appears far from random and, as we shall show shortly, is characterized by a well-defined average periodicity.

The second observation is related to the surprising magnitude of these fluctuations. It can be seen that, for the sample measurements on the low speed edge of the shear layer, the instantaneous value of the velocity is well below that of the undisturbed free stream, a very high fraction of the time. The correspondingly symmetric behavior is found on the high speed side of the layer. It is perhaps difficult to account for this behavior without taking into consideration the vortical nature of the large structure that is apparent in the flow visualization photographs and motion pictures discussed in section 3. Evidently these fluctuations represent the potential flow induced by the large structures in their streamwise procession. These extend to the as yet unentrained fluid in the vicinity of the shear layer. With this picture in mind, one can also appreciate that the amplitude of the perpendicular velocity fluctuations (along the y-axis) would also be of the same order of magnitude. This latter component is, of course, more directly connected with the entrainment process.

The third observation is related to the large variability between successive records. Within the shorter record of figure 9a, four almost identical structures have evidently been convected past the measuring station. By contrast, within the longer record of figure 9b (identical conditions except for a higher minimum burst amplitude level in the LDV signal processor; see previous section) evidence

of various stages of amalgamation between structures can be inferred. For example, the peaks around 0.10sec and 0.20sec, and 0.75sec and 0.85sec, suggest that a larger structure is in the process of formation by the amalgamation of two nearest neighbors. The time interval of approximately 0.10 sec between those two can be seen to be the characteristic period of the fluctuations for the data in both figures 9a and 9b. Closer inspection of the data record in figure 9b will also reveal evidence of other stages of the amalgamation process. The data record in figure 10 represents measurements taken 90 cm downstream of the splitter plate at a free stream velocity, on the high speed side, of U_1 = 330 cm/sec. A simple scaling calculation will reveal that the basic periodicity in this latter record is consistent with that of the previous two. The Reynolds number, based on U_1 and x, for the data in figure 10 is equal to 3×10^6 and is the highest at which quantitative data were recorded.

To examine the general periodic character of these data in a more quantitative fashion, the autocorrelation function of the velocity, given by

$$R_{uu}(\tau) = \overline{u'(t)\ u'(t+\tau)}\ ,$$

was computed for each record (see section 4).

Figures 11a, 11b, 11c and 11d represent the autocorrelation function of the streamwise velocity fluctuations, ensemble averaged over several records. The measurements were taken at the low speed edge of the shear layer at x = 15, 30, 60 and 90 cm downstream of the splitter plate. The free stream velocity, on the high speed side was U_1 = 165 cm/sec.

To render the similarity behavior of the fundamental periodicity more explicit, the time lag τ is scaled by the convection time

$$\tau_c = \frac{x - x_o}{U_c}$$

and plotted as a dimensionless variable

$$\frac{\tau}{\tau_c} = \frac{\tau U_c}{x - x_o} .$$

U_c is the convection velocity for the large structure, closely approximated by

$$U_c \simeq \frac{1}{2}(U_1 + U_2) \qquad (9)$$

for a shear layer of uniform density. The resulting values of the autocorrelation function are scaled by $(\frac{1}{2}\Delta U)^2$, where ΔU is the velocity difference across the shear layer ($\Delta U \equiv U_1 - U_2$). Note that $R_{uu}(0) = \overline{u'^2}$. A perfectly coherent sinusoidal velocity fluctuation whose upper and lower amplitude limits are given by U_1 and U_2 possess an autocorrelation function which, scaled in this fashion, is a cosine oscillating between $\pm$ 1.0. The plotted error bars represent the standard deviation of the ensemble averaged values of the autocorrelation function for each value of $\tau U_c/(x - x_o)$. The magnitude of these error bars is not the result of measurement uncertainties or computational errors but rather a measure of the variability between autocorrelation functions computed from consecutive data records. To illustrate this point, six estimates of the autocorrelation function, computed from data records of measurements taken at x = 30 cm, are plotted in figure 12. The curve in figure 12 labeled by the crosses (+) is computed from the data in figure 9b. Each curve appears smooth and well defined,

yet both the period and amplitude of the calculated autocorrelation functions can be seen to vary over a large range of values. A discussion of this important aspect of the data will be presented later on.

The most notable feature of the computed autocorrelation functions is that the fundamental periodicity of the velocity fluctuations appears consistent with the expected similarity scaling. If we define the fundamental period τ_o as twice the time lag to the first minimum of the autocorrelation function, we would expect that, for a given U_1/U_2 ,

$$\frac{\tau_o U_c}{x - x_o} = \text{const.}$$

for all x, U_1 and U_2. All the estimates of this quantity, resulting from measurements at $U_1 = 31.4, 165, 330$ cm/sec and $x = 15, 30, 60, 90$ cm at both the low speed and high speed edge of the shear layer are consistent with the inequality ($U_1/U_2 \simeq 5$)

$$0.40 < \frac{\tau_o U_c}{x - x_o} < 0.50 \quad . \tag{10}$$

The spacing between the structures, given by

$$\ell = \tau_o U_c \ , \tag{11}$$

is more appropriately scaled by the local vorticity thickness $\delta_{(\omega)}$, defined in terms of the maximum slope thickness of the mean velocity distribution, i.e.,

$$\frac{1}{\delta_{(\omega)}} \equiv \left(\frac{1}{\Delta U} \frac{\partial U}{\partial y}\right)_{max} .$$

Using the experimentally determined range of values for δ_ω, we have

$$3.1 < \frac{\tau_o U_c}{\delta_\omega} < 5.0, \qquad (12)$$

in reasonable agreement with the values inferred by Brown and Roshko (1974) from the data of Spencer and Jones (1971; $\tau_o U_c/\delta_\omega \sim 3.8$) and Winant and Browand (1974; $\tau_o U_c/\delta_\omega \sim 3.3$), and also consistent with the stability criterion for a single vortical structure of Moore and Saffman (1975), given by equation 2. Basing their argument on the stability of a vortex in the presence of the distorting field of its neighbors, these authors derive a stability criterion for a single structure that requires

$$\ell \geq 3.5\ \delta_\omega,$$

where ℓ is the spacing between vortices and δ_ω is the local maximum slope thickness.

The agreement of the fundamental period between measurements at the low speed edge and the high speed edge is worth noting. The local velocities there differ by almost a factor of five. It would be very difficult to explain an Eulerian frequency that is the same on both sides without recognizing the existence of a structure whose dimensions are of the order of the full shear layer width and which moves as a unit with a convection velocity of its own.

The second result that emerges from these data is related to the surprisingly long correlation times associated with the structure dynamics. The autocorrelation function retains its oscillatory character for time lags that are longer than any obviously relevant time scale.

The large structures amalgamate and disappear as identifiable entities, within a distance of the order of their mutual separation (Brown and Roshko 1974), and maintain a spacing proportional to $(x-x_o)$, on the average. One would not expect any coherence beyond the identifiable lifetime of each structure. Consequently, the oscillations in the auto-correlation function should have decayed after, at most, two structure periods corresponding to

$$\frac{\tau U_c}{x - x_o} \leqslant 1 \qquad (13)$$

(see equation 10). Since $(x - x_o)/U_c$ is also the convection time required for a disturbance associated with the large structure to traverse the distance x, the upper bound given by inequality 13 is the largest obvious time scale for the problem. Yet, within the experimental confidence limits, the data suggest the existence of memory times much longer than these upper bounds. It is as if the large structure phase is not completely destroyed in the amalgamation process, but remains coupled to the phase of the subsequently formed structures.

The third notable feature of the computed autocorrelation functions is related to the decrease in the standard deviation of the ensemble averages, as x increases. The autocorrelation functions computed from each record of measurements at the farthest downstream location agree reasonably well with each other. This is in marked contrast to the estimates for the measuring stations closer to the splitter plate, an example of which is shown in figure 12. In this respect, similarity scaling appears totally inadequate in explaining the dependence on x of the variability in the estimates of the autocorrelation functions.

It is perhaps surprising that the well-defined oscillations in the autocorrelation function estimates have not been found previously. Several reasons may be responsible for this discrepancy. The most important of these, we believe, is the choice of the location of the measuring station. The velocity fluctuations were measured just outside the turbulent region of the shear layer ($|\eta - \eta^*| \sim \frac{1}{8}$). At this location, the rapid, high intensity, small scale fluctuations in the shear layer do not have any significant effect, the intervening fluid acting as something of a low-pass filter. The situation is akin to the case of the cylinder wake. The best place to observe the vortex shedding frequency is just outside the wake. Estimates of the autocorrelation function computed from measurements at the center of the shear layer ($\eta = \eta^*$) have amplitudes for short time lags about ten times larger than the ones in figures 11a, 11b, 11c, 11d. Even though the oscillatory nature for longer time lags can still be seen, it appears appreciably less well-defined. We believe that this is a computational difficulty corresponding to a broader spectrum and a much higher mean square fluctuation level. The quasi-periodic nature of the signal was still quite apparent when the velocity measurements were plotted directly versus time. A more detailed study was not undertaken because of data acquisition limitations at the time. Recent improvements, however, will allow measurements in the turbulent region for the purposes of clarifying these issues and investigating the small scales.

6. The Effect of the Initial Conditions

There is a growing body of evidence that suggests that the initial conditions of the shear layer may also be important in determining the growth rate of the linear region. There is reason to believe for example that the 30% difference in the growth rate measured by Liepmann and Laufer (1947) and Wygnanski and Fiedler (1970) may be attributable to a tripping device placed in the boundary layer by the latter, upstream of the (real) origin of the shear layer. Batt (1975) could reproduce the Liepmann and Laufer (1947) data or the Wygnanski and Fiedler (1970) data by tripping or not tripping the boundary layer in the same apparatus.

A possible explanation of the importance of the initial conditions may lie in an analysis by Winant (1972) of the shear layer growth, on the basis of the vortex pairing mechanism, who concludes that the details of the initial vorticity distribution within the structures and the irregularities in the initial lateral displacement of the vortices have a definite effect on the subsequent growth rate.

The situation is well summarized by the collection of data in figure 10 of Brown and Roshko (1974), where growth rates measured by several experimenters are plotted as a function of the dimensionless ratio $\lambda = (U_1-U_2)/(U_1+U_2)$. If similarity reasoning is applicable, the shot gun appearance of the plotted points, within a relatively wide band of values, is something of an embarrassment. Nevertheless it is not possible to say, as of this writing, whether this departure from similarity is the result of the persistence of the effects of the initial conditions or experimental difficulties in generating a truly self-preserving shear layer. The

latter difficulty could be a consequence of the very large dimensions required. The two possibilities are, of course, not necessarily mutually exclusive.

Bradshaw (1966), in his investigation of the transition region of the shear layer, concluded that a streamwise extent of as many as 1000 initial momentum thicknesses may be required before similarity can be attained. A similar estimate can be obtained if one requires that the large structure spacing be at least ten times larger than the spacing of the initially amplified disturbance (Roshko 1974). This condition could, in fact, explain the large difference in the variability of the autocorrelation functions computed for a U_1 = 165 cm/sec at 15 cm and 30 cm downstream of the splitter plate (figures 11a and 11b), and the measurements further downstream. In this case, one thousand momentum thicknesses corresponds to x = 40 cm. It is interesting to note that the mean large structure spacing seems to have attained its self-preserving value as early as 15 cm downstream of the splitter plate.

It may be, however, that the estimate of a thousand momentum thicknesses, for full similarity to be attained, is actually low. This becomes plausible if we consider the large structure amalgamation scaling. If we assume that the spacing between large structures doubles after each interaction, then the number of interactions (tearings, pairings, etc.) contained between the shear layer origin and x, is given by

$$m(x) = \log_2 \left(\frac{x}{\ell_o}\right), \qquad (14)$$

where ℓ_o is the spacing of the initial disturbance. One thousand momentum

thicknesses corresponds to a value of m between 3 and 4, hardly a large number. Efforts to allow the shear layer to "forget" the initial conditions by a large downstream extent should be evaluated in terms of the sobering scaling of equation 14. The expected total number of interactions in this experiment (for U_1 = 165 cm/sec) within the effective test section of

$$0 < x < L \sim 2 \text{ meters}$$

is approximately given by $m(L) \sim 6$.

A second factor which would be expected to play a role is related to the distribution of vorticity within the large structure. There is reason to believe that it affects the dynamics of the large structure growth and amalgamation (Winant 1972, Moore and Saffman 1975). A shape parameter β can be defined in terms of the radius of gyration r_G of the vorticity distribution

$$r_G^2 \equiv \frac{1}{\kappa} \iint r^2 \omega(r, \phi)\, r dr d\phi, \qquad (15a)$$

where κ is the total circulation

$$\kappa \equiv \iint \omega(r, \phi)\, r dr d\phi\ . \qquad (15b)$$

The shape parameter β is then defined as

$$\beta \equiv \frac{2r_G}{\delta}$$

where δ is the diameter of the structure (cf. δ_{viz} of Brown and Roshko 1974), and is a measure of the concentration of vorticity within the structure (β = 0 corresponds to a point vortex). A "young" structure in the layer, the result of one or two amalgamations (small m), will have a

vorticity distribution closely related to the initial conditions and possibly different from that of an "old" structure which has been formed as the result of several amalgamations (larger m). Consequently, in a finite apparatus, the "linear" growth rate, for a shear layer of uniform density, would be a function of both U_1/U_2 and the vorticity distribution parameter β, i.e.

$$\frac{d}{dx}\,\delta_\omega(x) \sim f\left(\frac{U_1}{U_2}\,;\,\beta\right) . \qquad (16)$$

For a given set of initial conditions, the value of β, corresponding to a structure at x, would primarily depend on m, the structure "age." The notion of the "age" of a vortical structure was introduced by Owen (1970) who found a correlation between the behavior in the decay of aircraft trailing vortices and a logarithmic measure of the vortex lifetime.

Thus the growth rate, which depends on the slowly changing shape parameter would, in turn, also change slowly. The logarithmic dependence of m on x, however, could easily have caused such an effect to have escaped detection within the extent of any single apparatus. This is quite plausible since, in turn, the dependence of the growth rate on the vorticity distribution shape parameter β is probably also a weak one. For a fixed measuring station, however, the effect of changing β by adding a "tripping" wire could easily be noticeable (Batt 1975).

For a boundary layer that is initially laminar, the value of the initial structure spacing ℓ_o is of the order of ten boundary layer thicknesses. A tripping wire, depending on the Reynolds number based on its own dimensions, may introduce length scales many times smaller. As a result, the vorticity distribution within the structure at the downstream

measuring station could change because both the initial vorticity distribution would be altered and the "age" m would increase due to the decrease in ℓ_o.

These considerations suggest that the assumption that the initial conditions do not play a role in the downstream development of the "linear" growth region may not be a valid one. The initial conditions may have an effect persisting for many logarithmic increments downstream by determining a shape factor on which, in turn, the growth rate depends weakly. If this is correct, the shear layer may be characterized by a "linear" growth rate not because the initial conditions are forgotten so quickly but because they are forgotten so slowly. The "linear" growth region should then be viewed as being defined not only in terms of a velocity ratio U_1/U_2 but also in terms of a weak dependence on such slowly changing characteristics as the distribution of vorticity within the large structure which is largely determined by the initial conditions.

7. The Long Time Scales

The conjectures in the preceding section, if proven correct, could explain much of the apparent departure from similarity of the data available to date on the shear layer. They could not, however, explain the long memory time scales that were found in the autocorrelation functions, discussed in section 5.

The large variability in the autocorrelation function estimates from the records corresponding to the measurements closer to the splitter plate could be explained by the presence of characteristic times that are longer than those consistent with local scaling [i.e., $(x-x_o)/U_c$]. The fact that this variability does not appear in the measurements farthest from the splitter plate raises the possibility that time scales related to the total length of the apparatus are important.

For the structures at the furthest measuring station (90 cm downstream of the splitter plate trailing edge) only one more amalgamation is expected before the end of the test section ($\sim$ 200 cm before wall effects are important). That means that characteristic times that are at most twice the local period can be found in the corresponding velocity fluctuations. Measurements recorded at this location, spanning a total of many local structure periods have exhausted in some sense the possibilities in the velocity fluctuations. Consequently, estimates of the autocorrelation function computed from these records would be expected to be closer to the infinite time average for the process. In more conventional terms, in the problem of determining the spectrum for the process, each data record at larger x is much longer than the reciprocal of the lowest frequency present. If a mechanism exists that

can couple the longer periods of the downstream structures with the dynamics of the velocity fluctuations closer to the splitter plate, this would not be the case for the measurements at smaller x's. Recall that the records span time intervals proportional to x. At each measuring station, the record lengths were adjusted to include a given number of the (local) large structure cycles.

The existence of such a coupling scheme can be argued as follows. By considering the induced mean velocities outside the shear layer, we deduce that the ratio of the circulation around each vortical structure to the structure spacing must be given by

$$\kappa/\ell = \Delta U , \tag{17}$$

where ΔU is the velocity difference across the layer ($\Delta U \equiv U_1 - U_2$). The large structure spacing, however, increases in proportion to x (Brown and Roshko 1974, Winant and Browand 1974), i.e.,

$$\frac{\ell}{x-x_o} = \alpha \sim \text{constant}$$

where, for this experiment, $0.4 < \alpha < 0.5$ (inequality 10). Consequently, the expected circulation around a vortical structure will also increase with x, i.e.,

$$\kappa(x-x_o) \sim \alpha \cdot \Delta U \cdot (x-x_o) . \tag{18}$$

Therefore, even though the influence of a distant vortical structure on a given point decreases inversely with distance (infinite channel), the strength of distant vortices increases linearly with the downstream coordinate, and the effect does not vanish as the distance to the vortical structure increases.

The surprising conclusion is that all the structures downstream of a given point in a subsonic shear layer can influence the dynamics of that point. This can provide the coupling mechanism required to explain the observed variability in the autocorrelation function estimates. This coupling can also increase the importance of the initial conditions by essentially providing a feedback that may drive or synchronize an initial instability with the downstream fluctuations. As the structure at the end of the test section leaves, it excites the next initial rollup and keeps it in phase with the existing structures in the test section. In this manner the phase coherence can be preserved over times longer than $(x-x_o)/U_c$. The longest time scale available (i.e., L/U_c) determines the lowest frequency that will be found in the spectrum computed from data taken anywhere in the channel.

A closely related effect has been reported by Roshko(1967) who measured the velocity fluctuations in the transition region of a shear layer generated by a rearward facing step. At a boundary layer Reynolds number of $Re_x \sim 2 \times 10^3$, he found that the periodic fluctuations in the initial stages of the transition region were strongly modulated by a much lower frequency, whose period is approximately ten times that of the local fluctuations. He speculates that the coupling synchronizes the oscillations in the location of the reattachment point, which are sustained by this feedback mechanism.

A more recent example of this feedback mechanism on the dynamics of the shear layer can be found in the experimental investigation of flow over a cavity (Sarohia 1975). In this case the free shear layer that originates at the upstream edge of the cavity reaches a self-similar

mean velocity profile within fifteen initial momentum thicknesses. The feedback from the downstream edge of the cavity, however, is so strong as to impose well defined resonant modes on the flow pattern. The shear layer over the cavity was found to grow linearly with x after fifteen initial momentum thicknesses but at a rate which was a function of the ratio L/θ_o, where L is the total length of the cavity and θ_o is the initial momentum thickness. The situation is, of course, not quite equivalent because, in most cases, the cavity was not long enough for any large structure amalgamations to have occurred. Nevertheless it is an example of a free shear layer where the finite extent of the layer plays an important role.

In view of this mechanism that couples the dynamics at a point in the shear layer to the structures downstream, the problem of a steady-state, subsonic, infinite shear layer must remain academic. An infinite shear layer would render the behavior of the fluid, at some station x, non-stationary in a stochastic sense. The feedback of ever decreasing frequencies from the downstream structures would make the estimation of the power spectrum of the fluctuations at x impossible in principle. In practice, of course, the effect of the downstream feedback is reduced by three dimensional effects (walls at $z = \pm \frac{1}{2} L_z$), or image flow (wall at $y = \frac{1}{2} L_y$ and/or $y = -\frac{1}{2} L_y$), so that the finite dimensions of the apparatus enter (logarithmically) to govern the dynamics. It appears, therefore, that an analysis of the behavior of a subsonic, two-dimensional shear layer cannot be local but must consider the full effect of the flow within the finite extent of the apparatus.

8. Conclusion

Using flow visualization techniques, it was possible to verify directly and record photographically and on motion pictures that the large structures, that were observed in the shear layer at lower Reynolds numbers, persisted to Reynolds numbers of $x\,U_1/\nu \sim 3\times10^6$. It was also possible to study the mechanism that eventually brings fluid elements originating from either side into intimate contact within the shear layer. It was found that the freshly entrained fluid is initially a part of the irrotational motion of the large structure and remains largely unmixed during the lifetime of the associated structure. Mixing is very rapid, however, once it begins and appears intimately connected with the amalgamation processes of the large structure. This was verified directly by labeling the fluid being entrained from the two sides with an acid and a base respectively, and observing the chemical reaction by the change in color of a pH indicator, premixed with the acid solution. It now appears that entrainment across the shear layer boundaries and fine scale mixing with the rest of the fluid within those boundaries are two almost distinct stages of the overall process.

Using laser Doppler velocimetry techniques, discrete measurements of the streamwise velocity component were made at the edges of the shear layer. From the computed autocorrelation functions of the streamwise velocity fluctuations, it was possible to assign a fundamental periodicity to the large structure that was found to be in accordance with the expected similarity scaling. Other quantitative features of the velocity data, however, do not appear consistent with expected similarity behavior and anticipated time scales. To explain these features and

shear layer published data from other sources, two hypotheses are formulated.

It is argued that, as a result of the logarithmic dependence of the number of large structure interactions (amalgamations) on the effective length of the shear layer, the initial conditions play an important role within the extent of any realizable experimental apparatus. Consequently, the growth rate of the shear layer and other related features are not expressible as universal functions of the classical dimensionless parameters, U_1/U_2, ρ_1/ρ_2, $M_1 \equiv U_1/a_1$, etc. Secondly, it is observed that whereas the induced velocity at a point in the shear layer, due to a vortical structure downstream, diminishes inversely as the distance to the structure, the strength (circulation) of the vortical structures increases in proportion to the distance between the structure and the shear layer origin. As a result, in a subsonic shear layer, all the structures downstream of a given point affect the flow at that point. Consequently, it becomes necessary to analyze the two-dimensional shear layer globally, taking into consideration the effects of the initial conditions and the finite extent of the flow apparatus.

9. Acknowledgments

Even though we should be considered responsible for the results and ideas presented here, we would like to think of this work as the direct outgrowth of the collective activity of the GALCIT Fluid Mechanics Group. We are particularly indebted to Professor Anatol Roshko for his advice, guidance and critical ear throughout the stages of the experimental work and data analysis. Many thanks are due to Dr. J. E. Broadwell, Professor D. E. Coles and Professor P. G. Saffman for many helpful arguments and assistance with the text. The success of the novel signal processing and data acquisition system is due, to a large extent, to the expert design and construction of the electronics by Mr. Daniel Lang. We would also like to thank Mr. Tom Ward for his cooperation and assistance in the operation of the GALCIT Free Surface Water Tunnel. One of us (P. E. D.) would also like to thank Professor I. J. Wygnanski for a short discussion in which he brought to our attention the results on the mixing layer growth by Batt (1975).

The work was supported by the Office of Naval Research (Fluid Dynamics Program Contract No. N00014-67-A-0094-0037 and Project SQUID Contract No. 4965-42) and the Caltech President's Fund Grant No. PF-075.

REFERENCES

D. O. Barnett and H. T. Bentley, III (1974), "Statistical Bias of Individual Realization Laser Velocimeters.", Proceedings of the Second International Workshop in Laser Velocimetry, Vol. I, 428-444.

R. G. Batt (1975), "Some measurements on the effect of tripping the two-dimensional shear layer.", AIAA Journal 13, 245-247.

P. Bradshaw (1966), "The effect of initial conditions on the development of a free shear layer.", J.Fluid Mech. 26, 225-236.

G. L. Brown and A. Roshko (1971), "The effect of density difference on the turbulent mixing layer.", Turbulent Shear Flows, AGARD-CP-93, 23-1 - 23-11.

G. L. Brown and A. Roshko (1974), "On density effects and large structure in turbulent mixing layers,", J. Fluid Mech. 64, 775-816.

P. E. Dimotakis and D. B. Lang (1974), "Single Scattering Particle Laser Doppler Velocimetry.", Bull. Am. Phys. Soc., Nov. 1974, 1145.

P. E. Dimotakis (1975), "Single Scattering Particle Laser Doppler Velocimetry.", submitted for publication to the Journal of Fluid Mechanics.

P. E. Dimotakis (1976), "Single Scattering Particle Laser Doppler Measurements of Turbulence.", submitted to AGARD Symposium on Non-Intrusive Instrumentation in Fluid Flow Research (Saint-Louis France, April '76).

H. W. Liepmann and J. Laufer (1947), "Investigations of free turbulent mixing.", NACA TN-1257.

W. T. Mayo Jr. (1970), "Spatial Filtering Properties of the Reference Beam in an Optical Heterodyne Receiver.", Appl. Optics 9, 1159-1162.

References (Cont'd)

D. K. McLaughlin and W. G. Tiederman (1973), "Biasing correction for individual realization of laser anemometer measurements in turbulent flows.", Phys. Fluids 16, 2082-2088.

D. W. Moore and P. G. Saffman (1975), "The density of organized vortices in a turbulent mixing layer.", J. Fluid Mech. 69, 465-473.

P. R. Owen (1970), "The Decay of a Turbulent Trailing Vortex.", Aero. Quarterly 61, 69-78.

A. Roshko (1967), "Transition in Incompressible Near-Wakes.", Boundary Layers and Turbulence, Phys. Fluids 1967 Supplement, S181-S183.

A. Roshko (1974), "Progress and Problems in Understanding Turbulent Shear Flows.", in "Turbulent Mixing in Nonreactive and Reactive Flows", S. N. B. Murthy, (ed.) Plenum Press, New York, 1975.

V. Sarohia (1975), Experimental and Analytical Investigation of Oscillations in Flows over Cavities, Ph. D. Thesis, Department of Aeronautics, California Institute of Technology (to be presented at the AIAA 14th Aerospace Sciences Meeting, January, 1976).

H. Sato (1956), "Experimental investigation on the transition of laminar separated layer.", J. Phys. Soc. Japan 11, 702-709, 1128.

A. E. Siegman (1966), "The Antenna Properties of Optical Heterodyne Receivers.", Appl. Optics 5, 1588-1594.

B. W. Spencer and B. G. Jones (1971), "Statistical investigation of pressure and velocity fields in the turbulent two stream mixing layer." AIAA Paper No. 71-613.

C. D. Winant (1972), Vortex pairing in a turbulent shear layer at moderate Reynolds numbers., Ph. D. Thesis, Department of Aerospace Engineering, University of Southern California, Los Angeles.

References (Cont'd)

C. D. Winant and F. K. Browand (1974), "Vortex pairing: the mechanism of turbulent mixing layer growth at moderate Reynolds number.", J. Fluid Mech. 63, 237-255.

I. Wygnanski and H. E. Fiedler (1970), "The two dimensional mixing region." J. Fluid Mech. 41, 327-361.

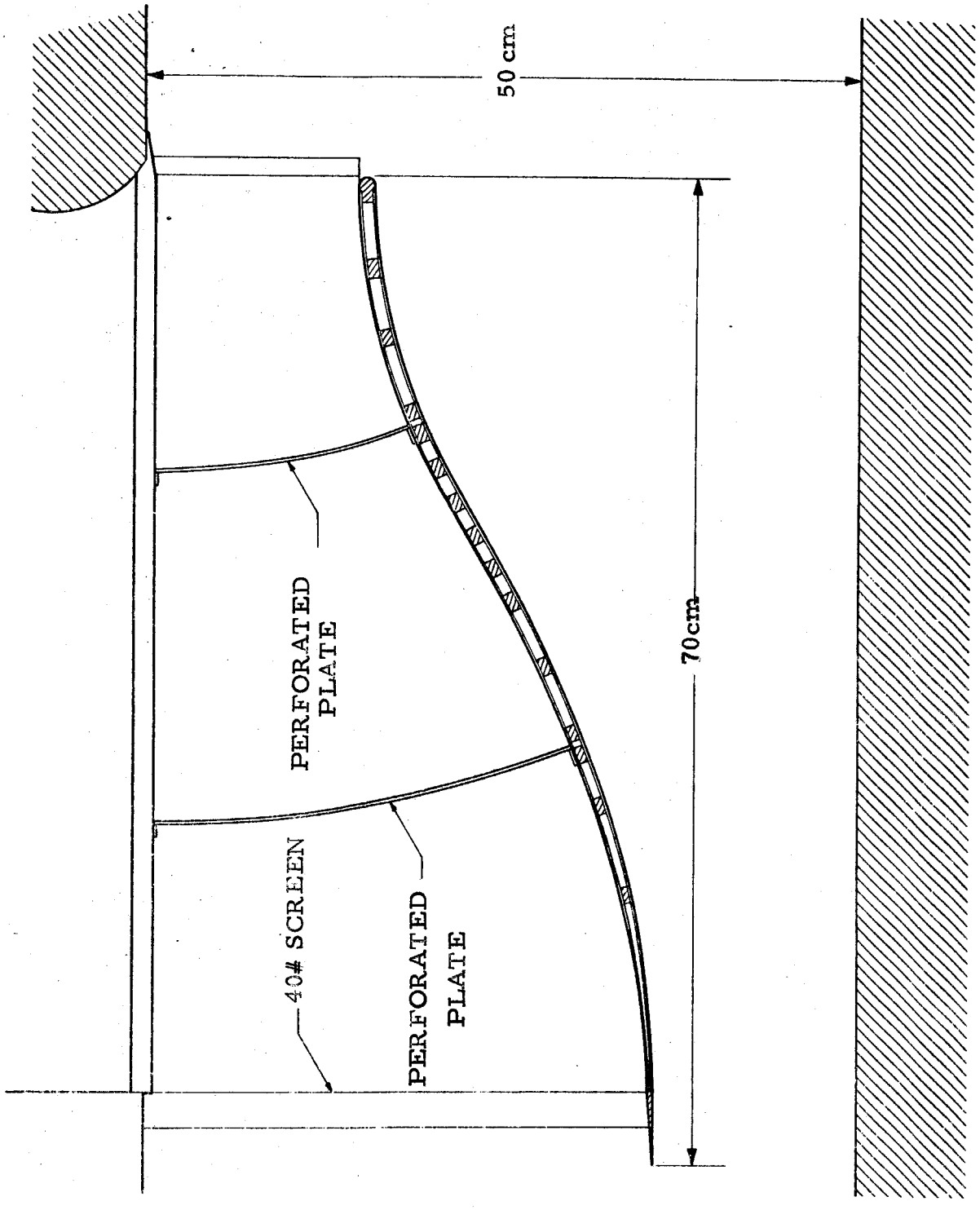

Figure 1. Insert for the 5:1 velocity ratio shear layer.

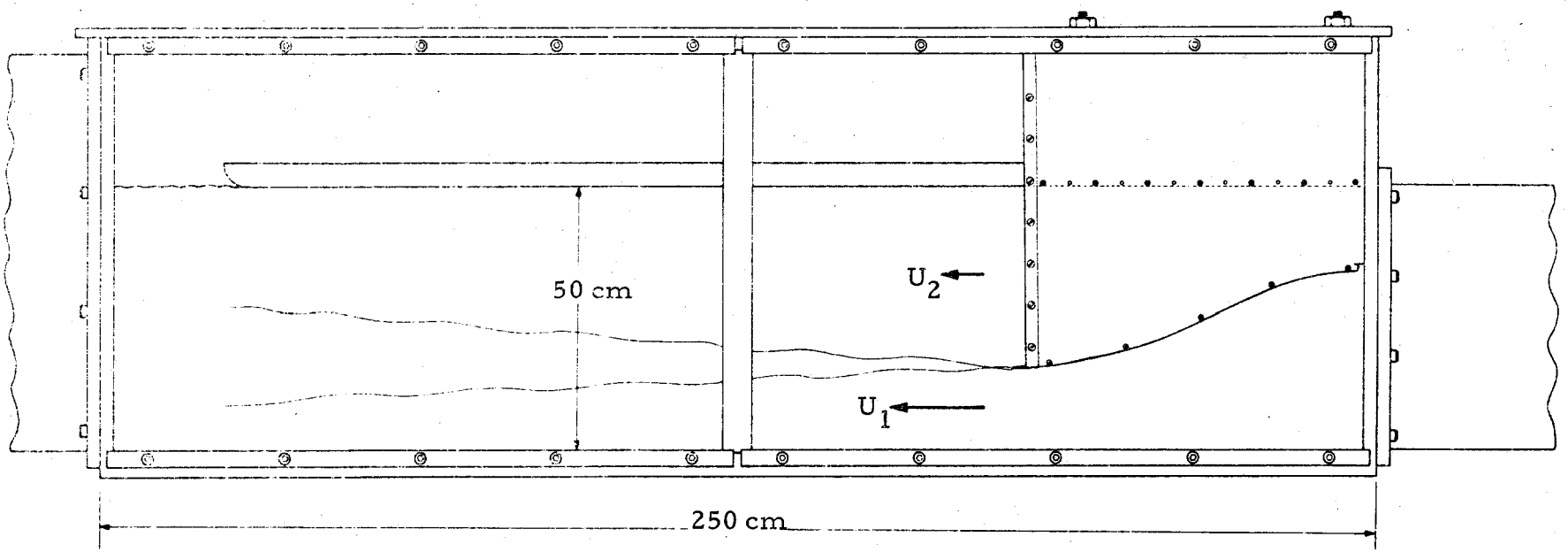

Figure 2. Test section with insert and top installed.

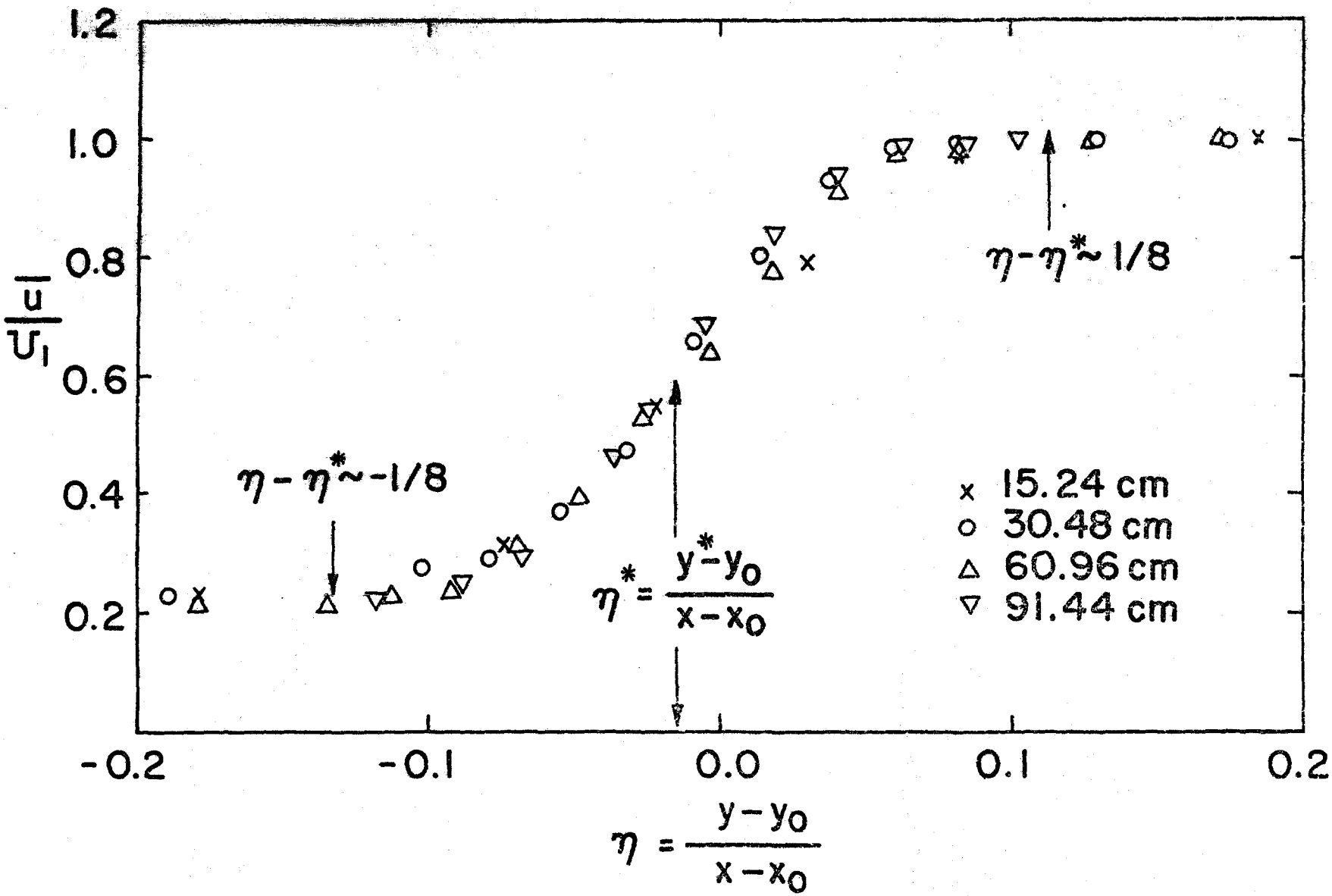

Figure 3. Similarity mean velocity profiles at x = 15.24 cm(X), 30.48 cm(0), 60.96 cm(Δ), 91.44 cm(▽), x_0 = 3.05 cm.

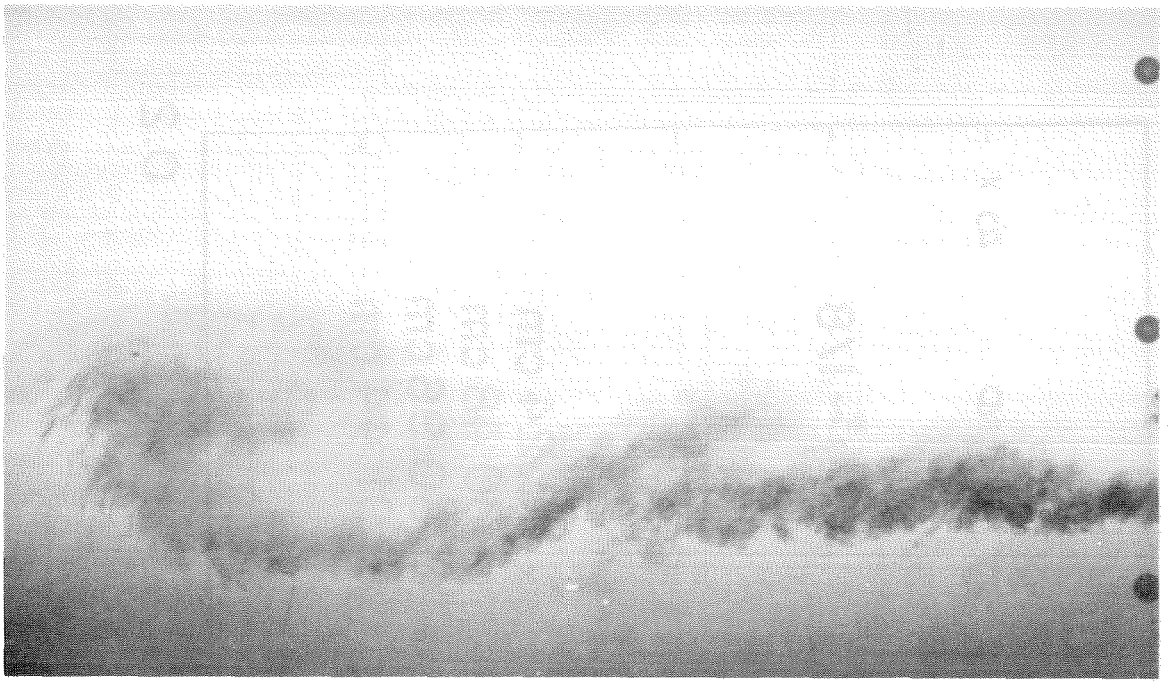

a) injection from high speed side

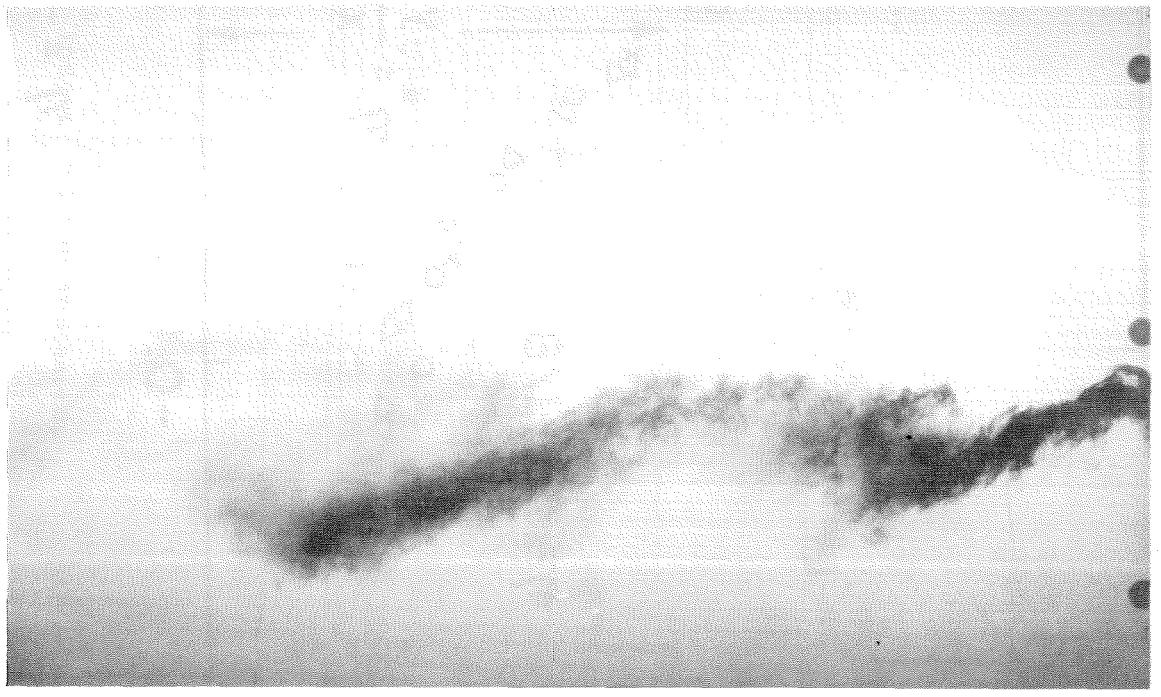

b) injection from low speed side

Figure 4. Large structure 120 cm(picture center) downstream of the splitter plate, $U_1 = 100$ cm/sec, flow from right to left, high speed side on the bottom.

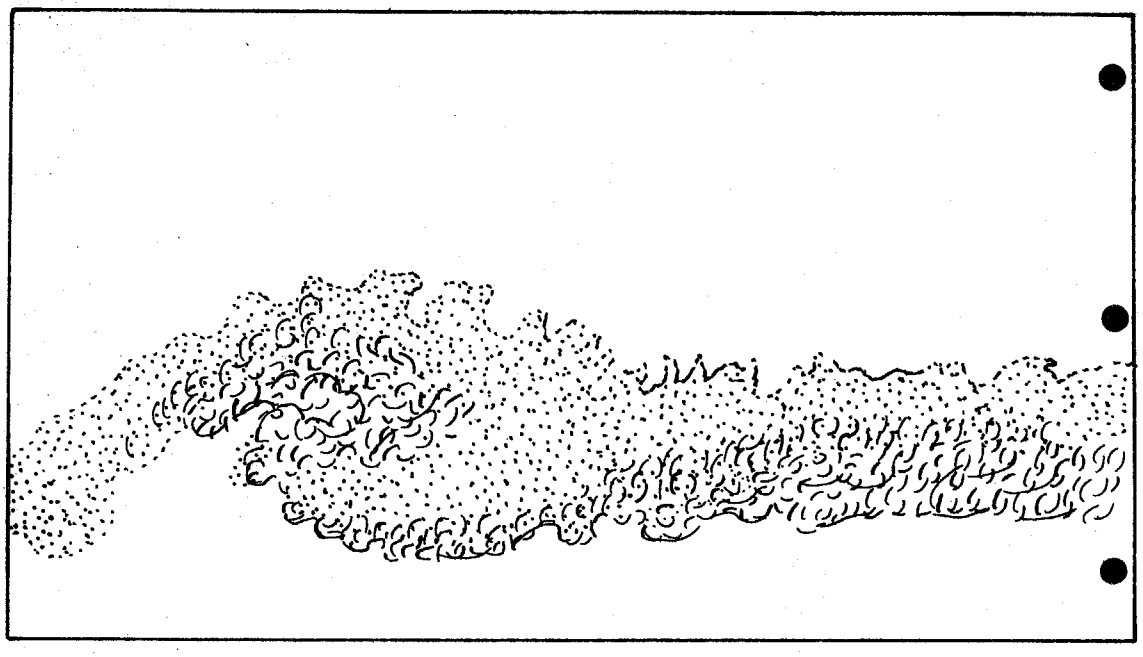

Figure 5. Flow as in figure 4. Simultaneous injection from both sides (upper side is the low speed side).

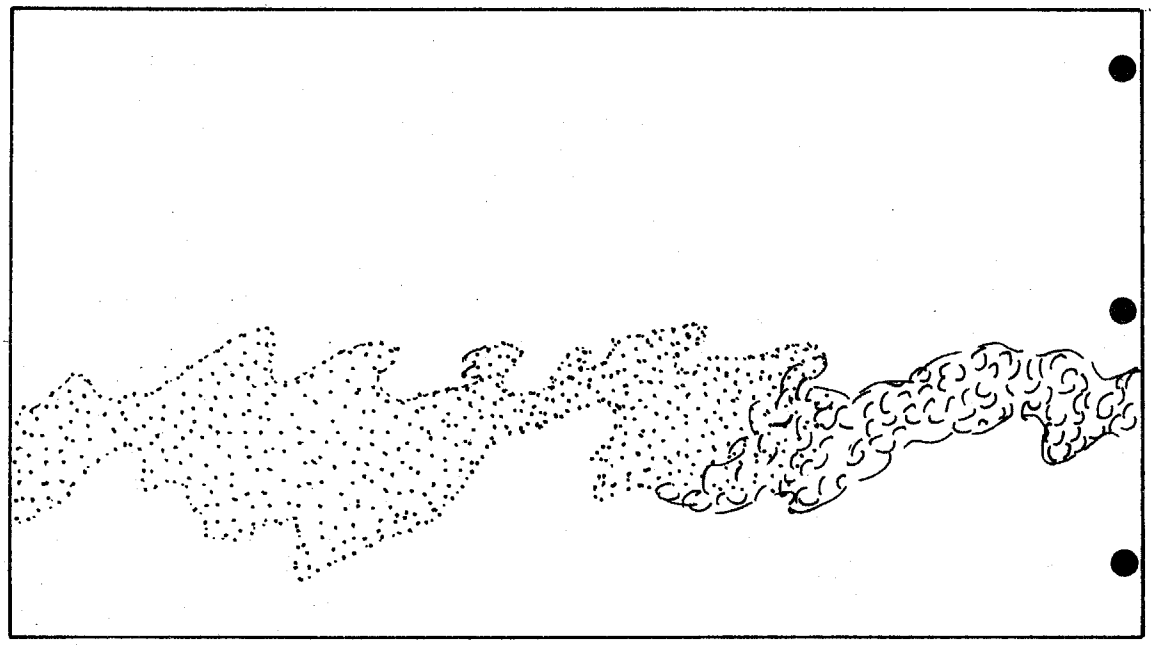

Figure 6. Flow as in figure 4. Chemical reaction.

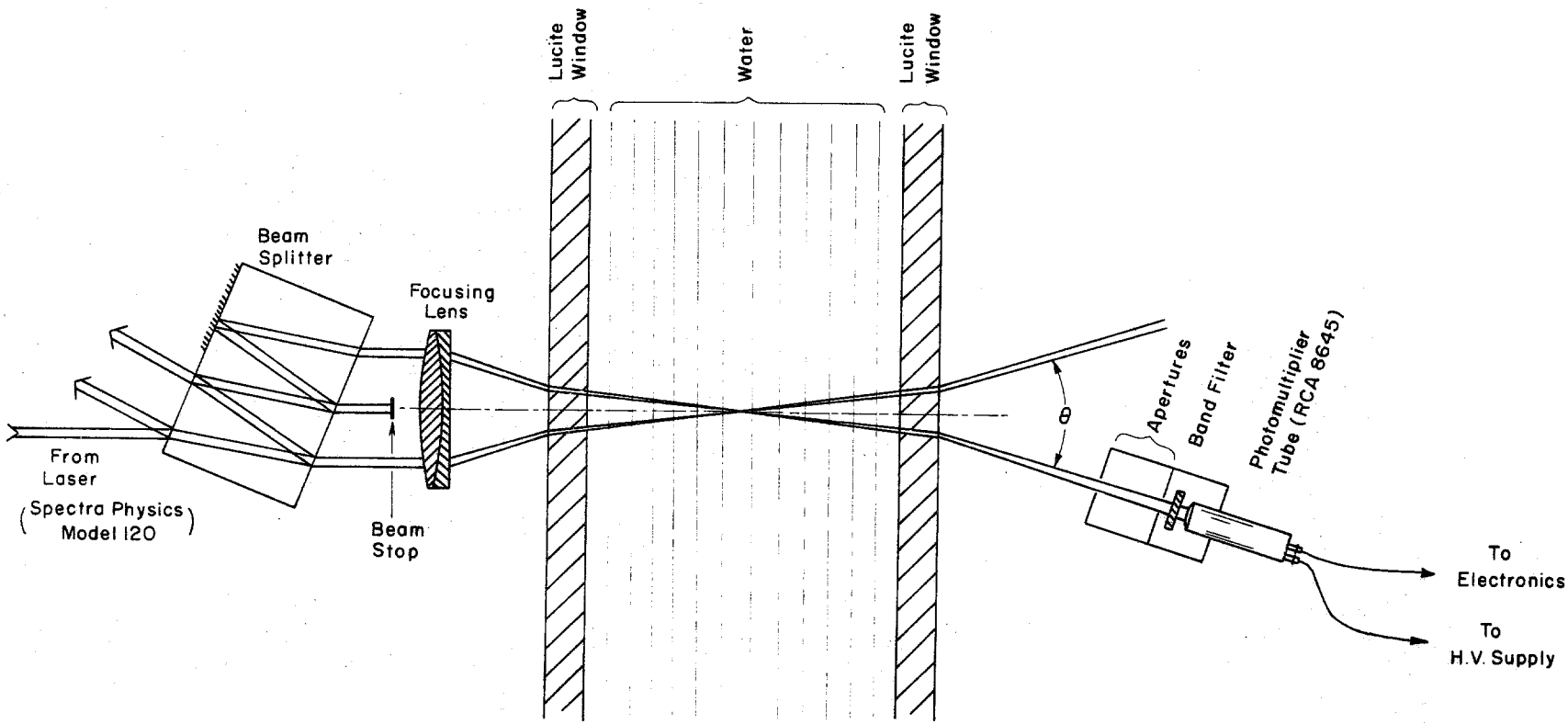

Figure 7. Laser Doppler reference-scatter optics.

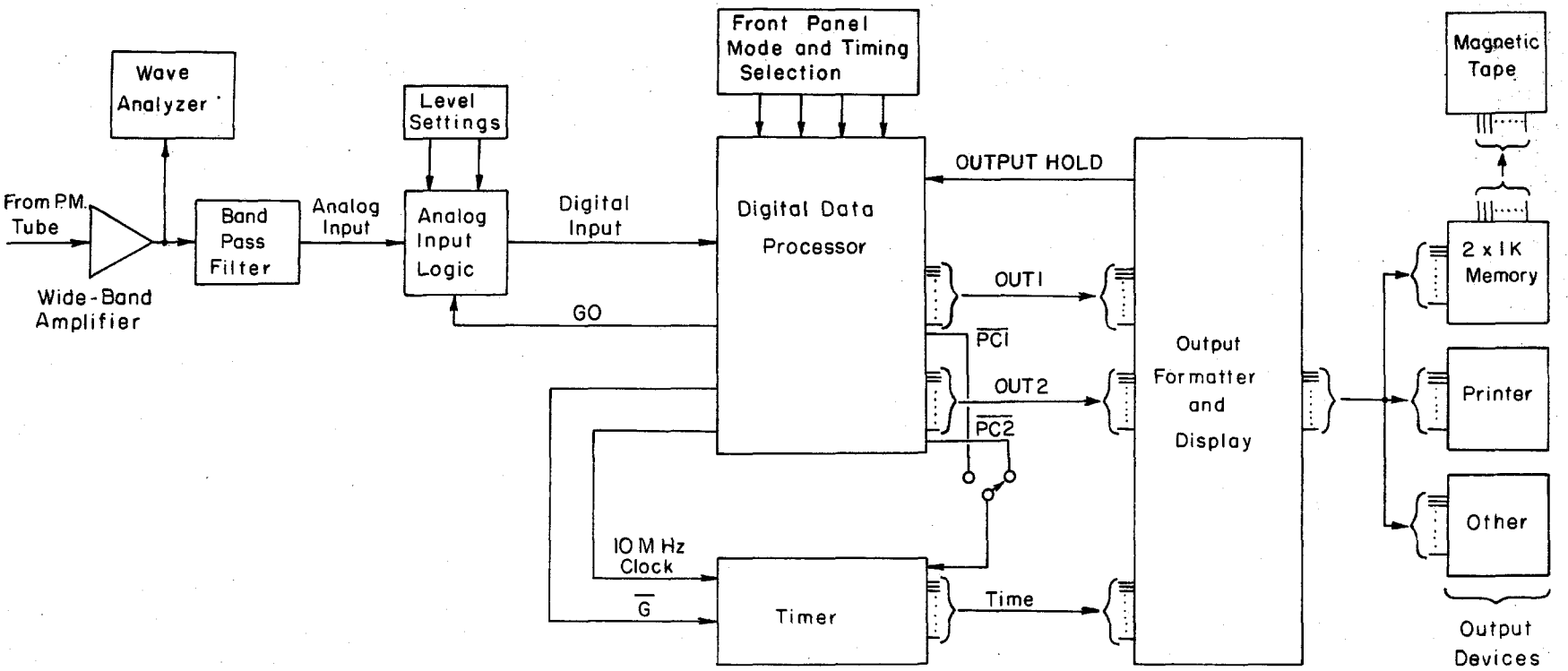

Figure 8. Signal processing and data acquisition system.

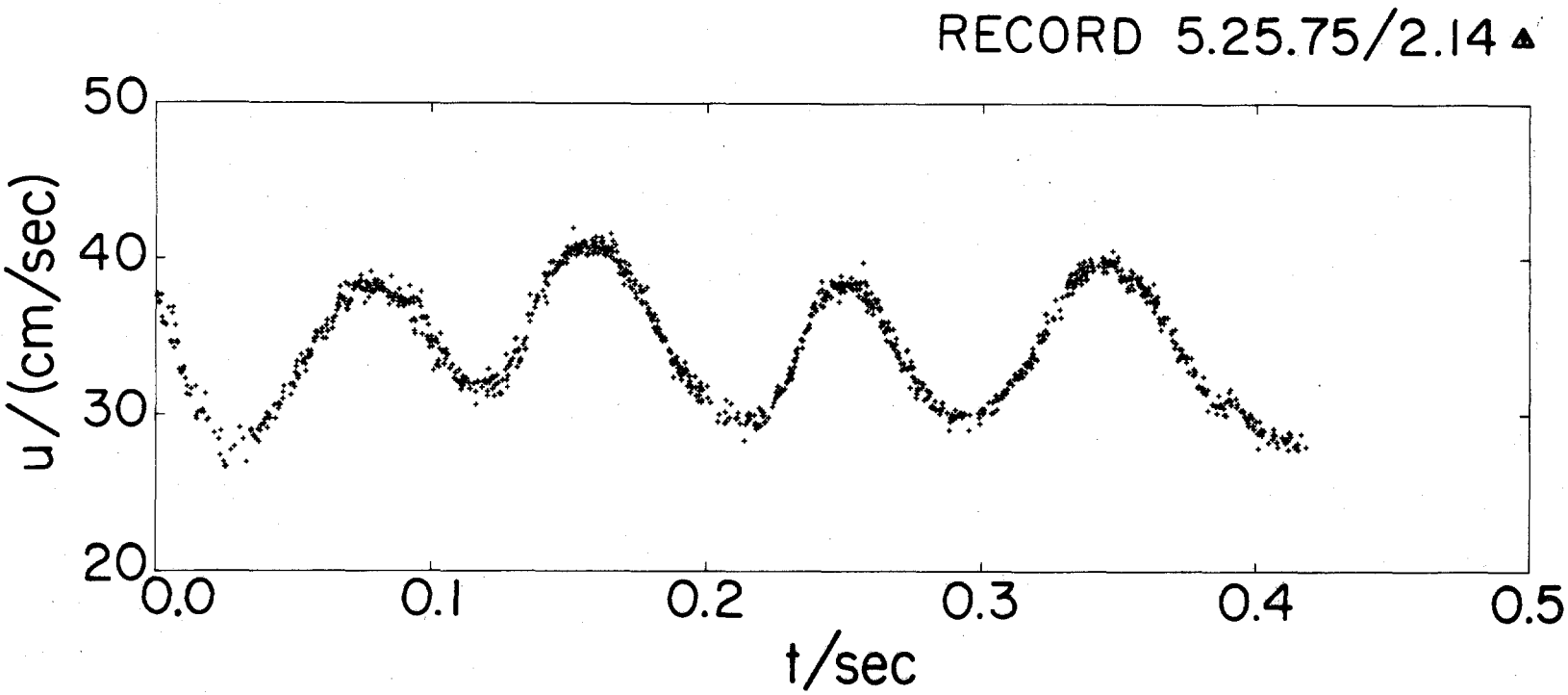

$U_1 = 165\,\text{cm/sec}$ $\quad x = 30.48\,\text{cm}$

$U_2 = 35\,\text{cm/sec}$ $\quad y = -3.53\,\text{cm}$

$$\eta - \eta^* = \frac{y - y^*}{x - x_0} = -1/8$$

Figure 9a. Velocity records taken at U_1 = 165 cm/sec, low speed edge. T = 0.419 sec.

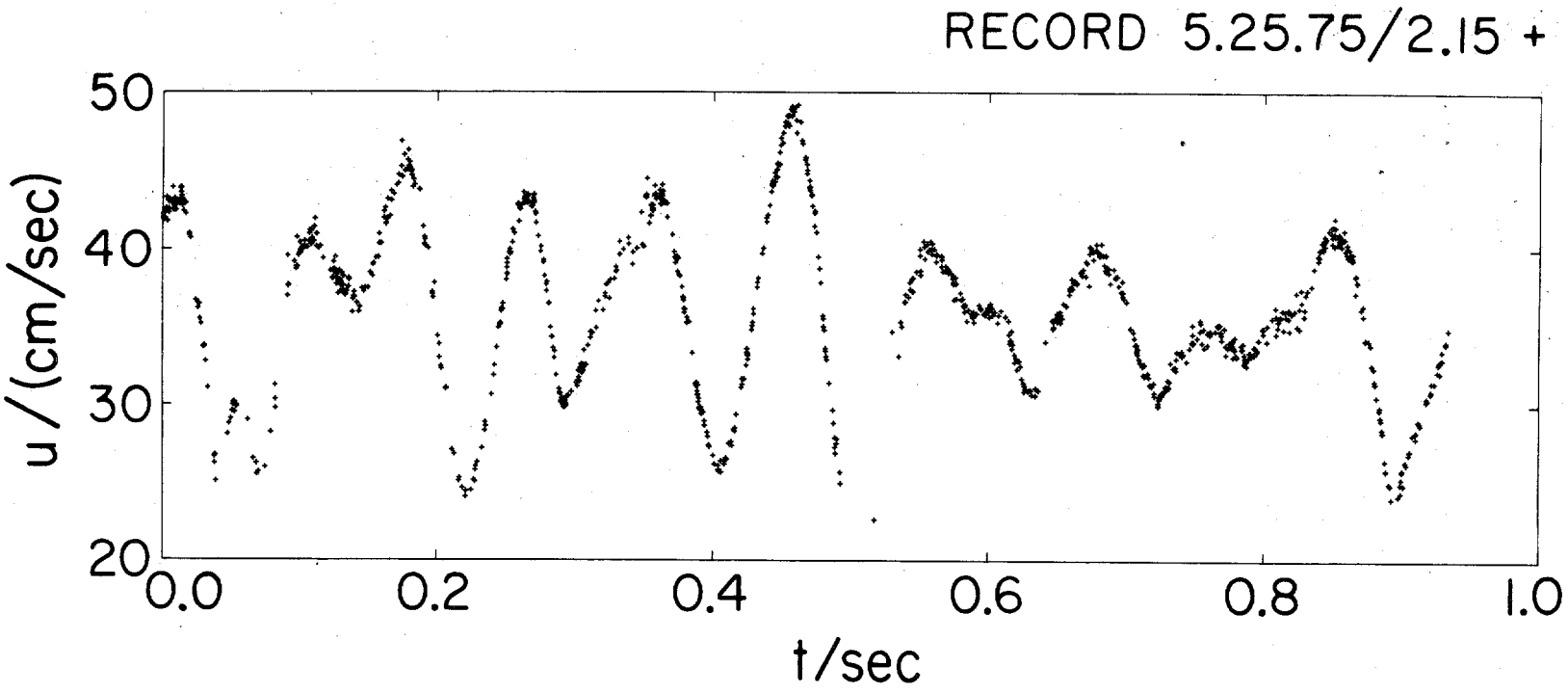

Figure 9b. Velocity records taken at U_1 = 165 cm/sec, low speed edge. T = 0.934 sec.

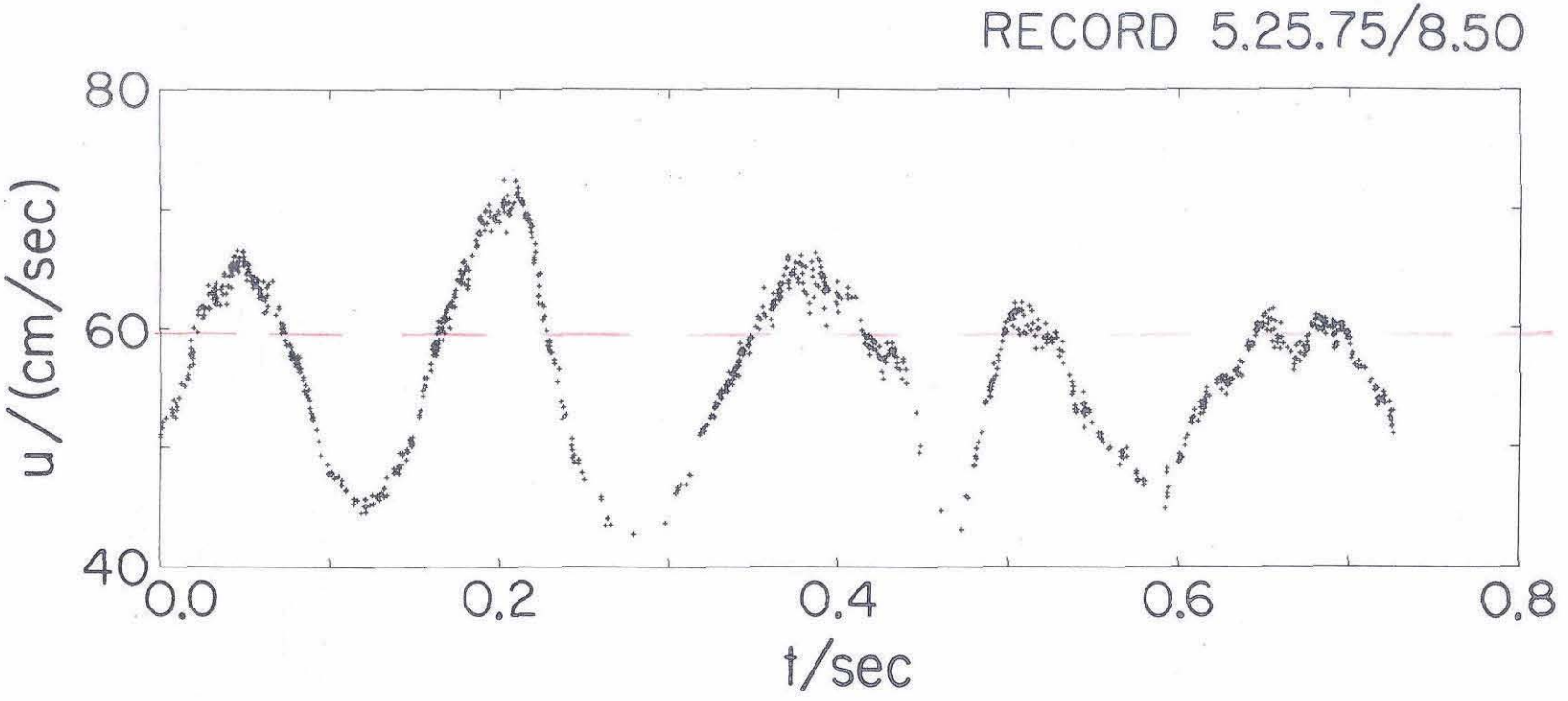

$U_1 = 330$ cm/sec $\qquad x = 91.4$ cm

$U_2 = 59$ cm/sec $\qquad y = -12.1$ cm

$$\eta - \eta^* = \frac{y - y^*}{x - x_0} = -1/8$$

Figure 10. Velocity record at shear layer low speed edge for $U_1 = 330$ cm/sec, $T = 0.726$ sec.

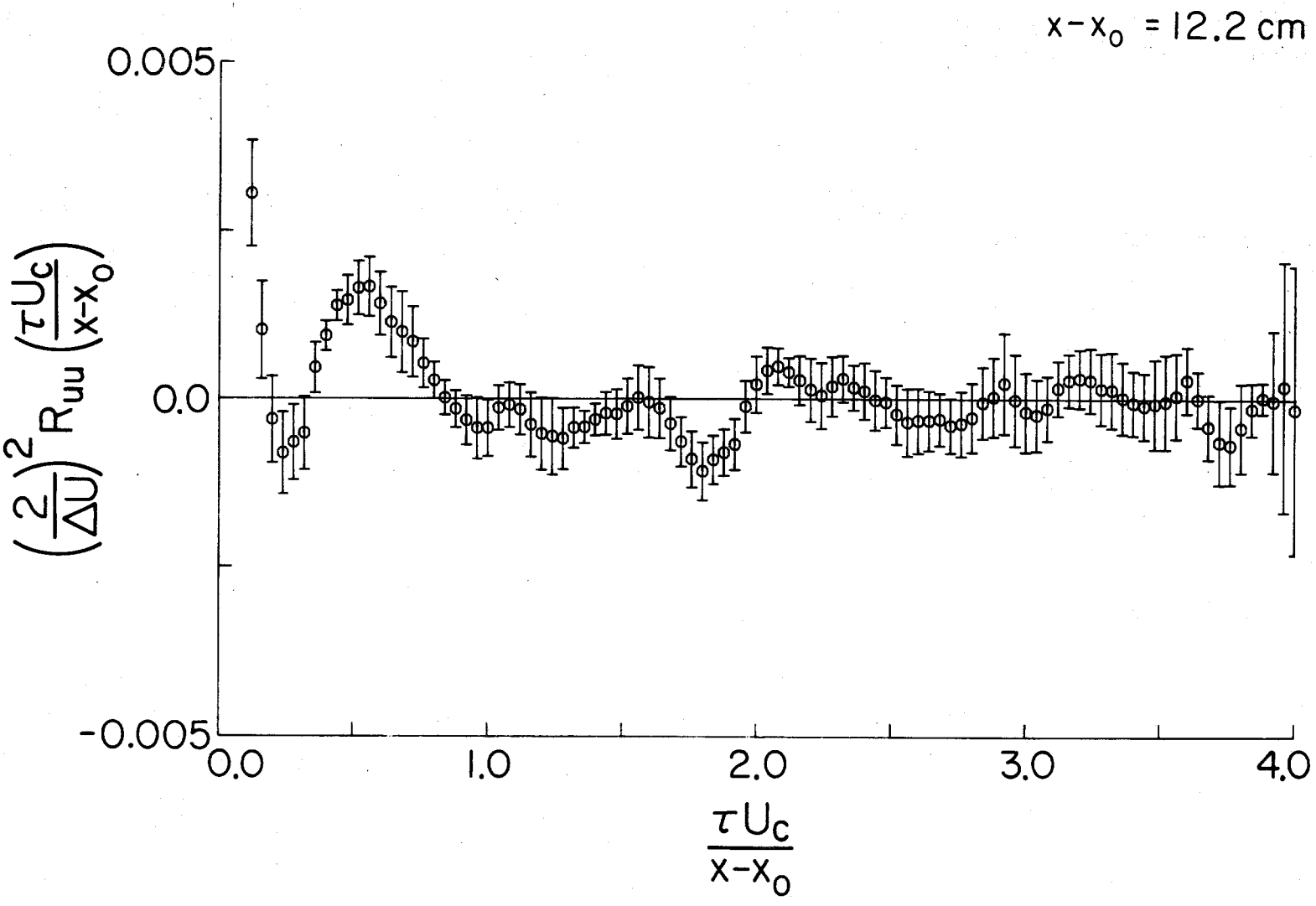

Figure 11a. Autocorrelation function. U_1 = 165 cm/sec, $\eta - \eta^* = -\frac{1}{8}$, x = 15 cm.

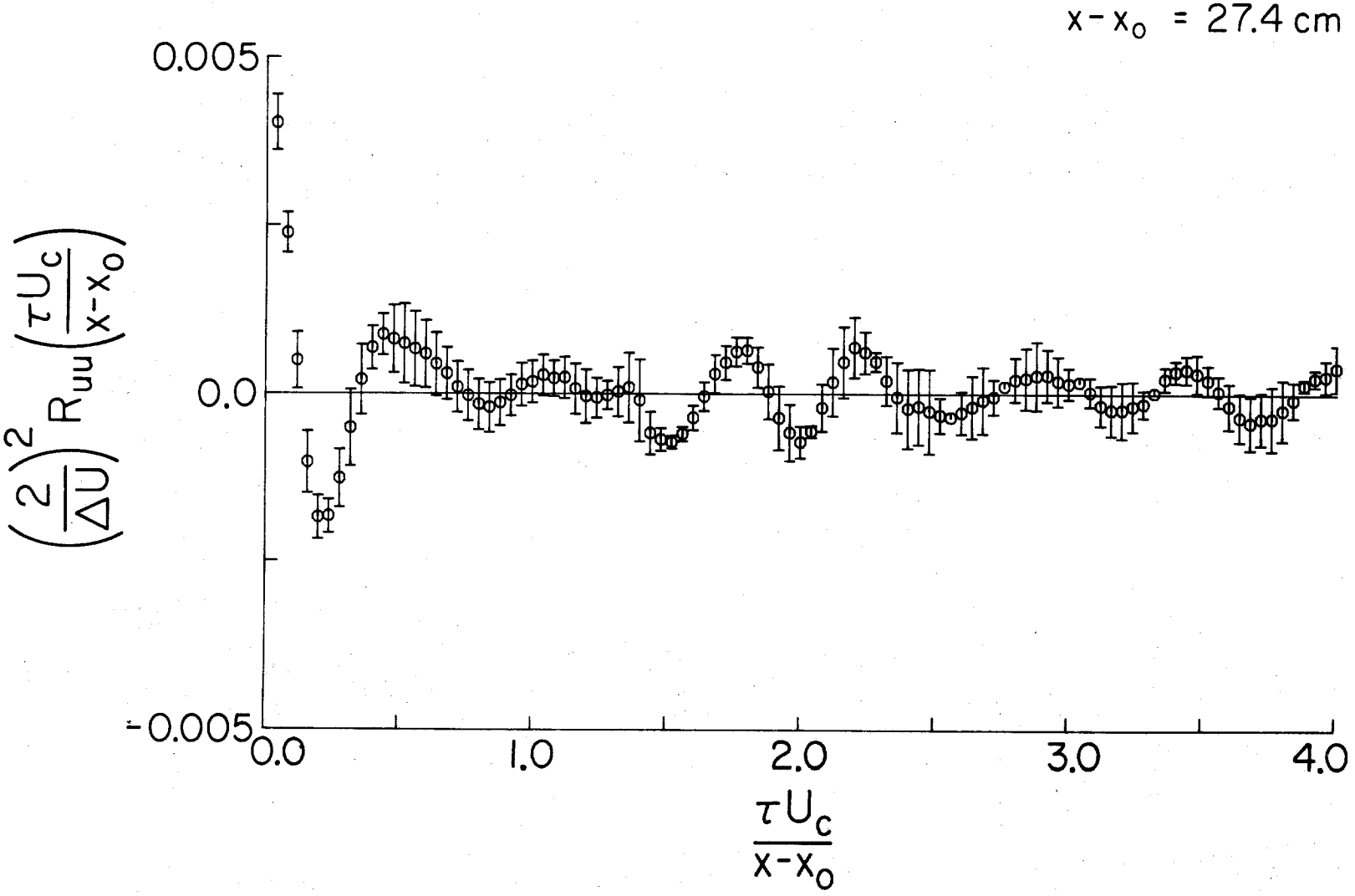

Figure 11b. Autocorrelation function. $U_1 = 165$ cm/sec, $n - n^* = -\frac{1}{8}$, $x = 30$ cm.

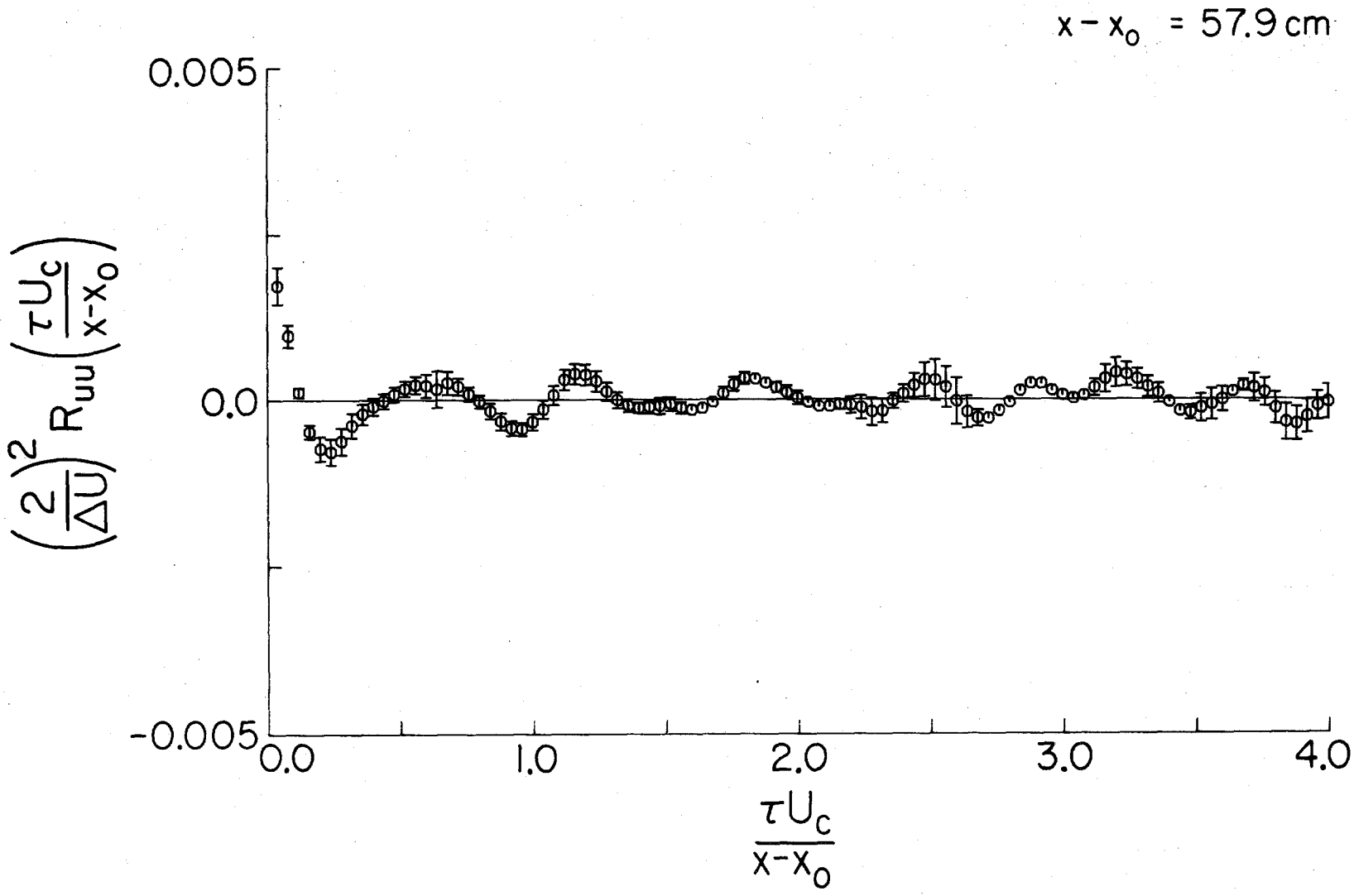

Figure 11c. Autocorrelation function. U_1 = 165 cm/sec, $\eta - \eta^* = -\frac{1}{8}$, x = 60 cm.

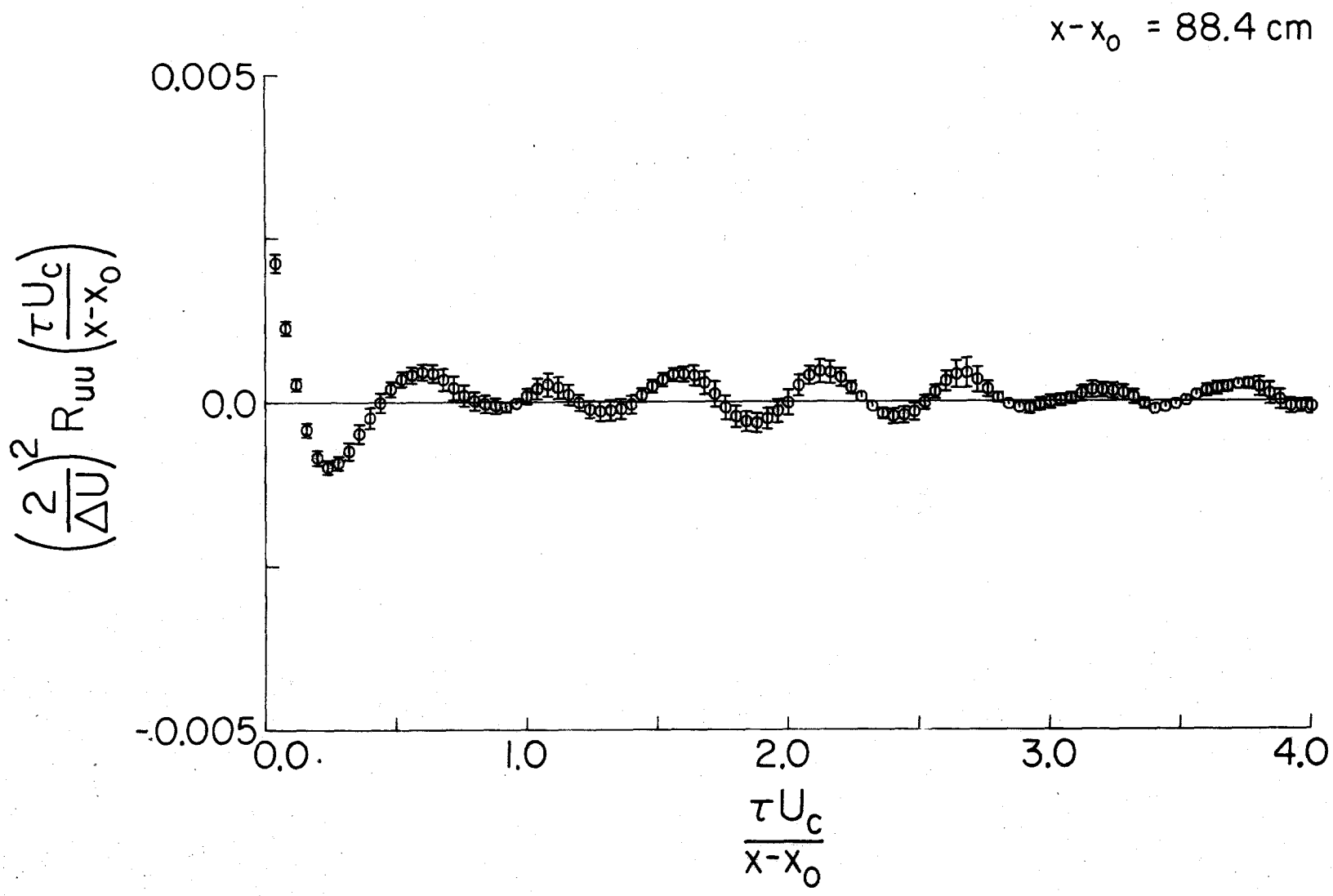

Figure 11d. Autocorrelation function. U_1 = 165 cm/sec, $\eta - \eta^* = -\frac{1}{8}$, x = 90 cm.

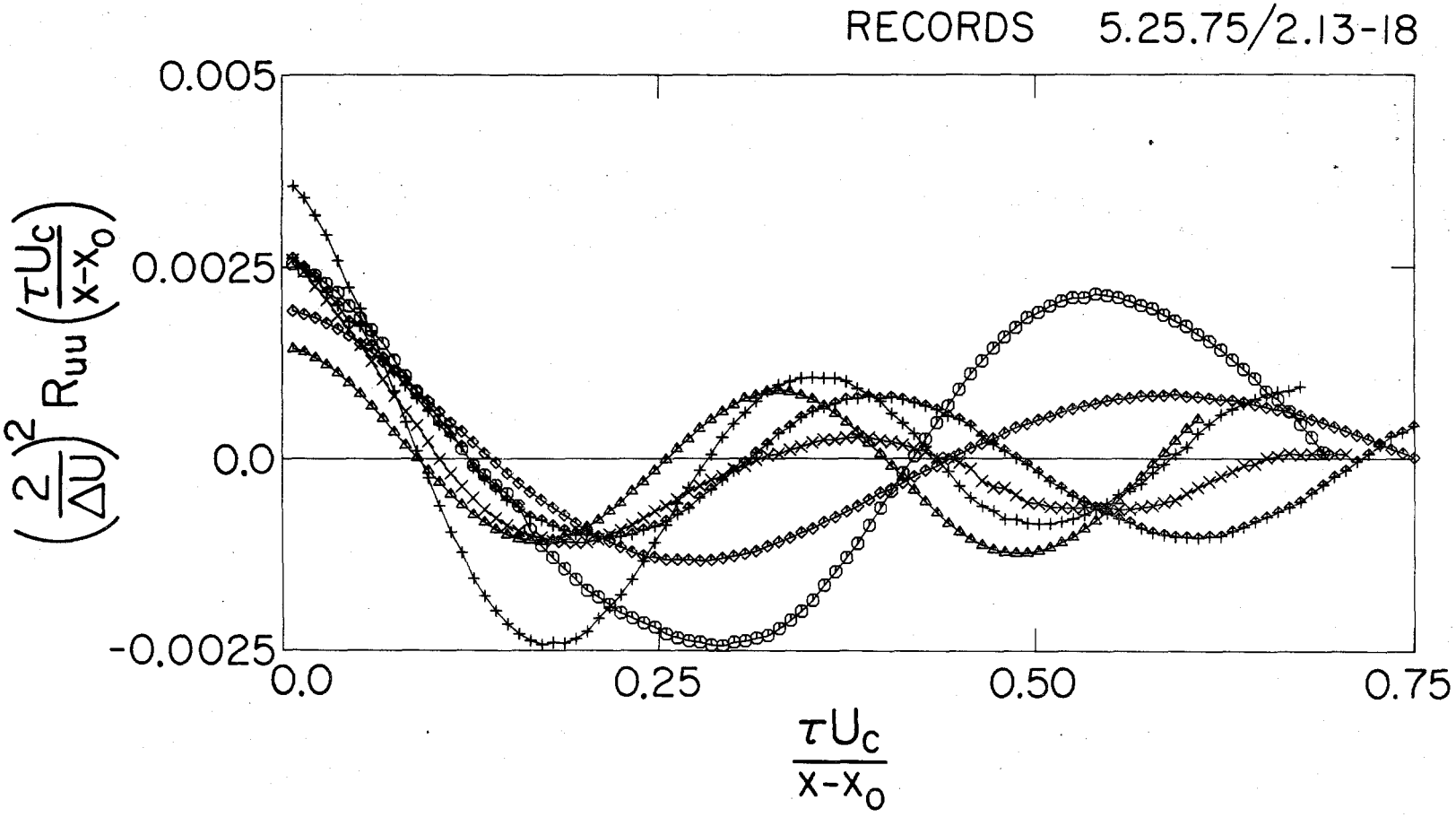

Figure 12. Six estimates of the autocorrelation function at U_1 = 165 cm/sec, x = 30 cm, $\eta - \eta^* = -1/8$.

GOVERNMENT AGENCIES

British Embassy
3100 Massachusetts Avenue, N.W.
Washington, D.C. 20008
ATTN: Mr. J. Barry Jamieson
Propulsion Officer

Central Intelligence Agency
Washington, D.C. 20505
ATTN: CRS/ADD/Publications

Institute for Defense Analyses
400 Army-Navy Drive
Arlington, Virginia 22202
ATTN: Dr. Hans G. Wolfhard,
Sen. Staff

Defense Documentation Center
Cameron Station
Alexandria, Virginia 22314

EPA Technical Center
Research Triangle Park
North Carolina 27711
ATTN: Dr. W. Herget, P-222

Esso Research and Engineering Company
Government Research Laboratory
P.O. Box 8
Linden, New Jersey 07036
ATTN: Dr. William F. Taylor
Senior Research Engineer

Arnold Air Force Station
Tennessee
ATTN: AEDC (DYF)

Arnold Air Force Station
Tennessee 37389
ATTN: R.E. Smith, Jr., Chief
T-Cells Division
Engine Test Facility

Air Force Aero Propulsion Laboratory
Wright-Patterson Air Force Base
Ohio 45433
ATTN: STINFO Office

Air Force Eastern Test Range
MU-135
Patrick Air Force Base
Florida 32925
ATTN: AFETR Technical Library

Air Force Office of Scientific Research
1400 Wilson Boulevard
Arlington, Virginia 22209
ATTN: Dr. Joseph F. Masi

Air Force Aero Propulsion Laboratory
Wright-Patterson AFB, Ohio 45433
ATTN: AFAPL/TBC
Dr. Kervyn Mach

Air Force Aero Propulsion Laboratory
Wright-Patterson AFB, Ohio 45433
ATTN: AFAPL/TBC
Francis R. Ostdiek

Air Force Rocket Propulsion Laboratory
Department of Defense
Edwards AFB, California 93523
ATTN: LKCG (Mr. Selph)

U.S. Army Air Mobility Research and
Development Laboratory
Eustis Directorate
Fort Eustis, Virginia 23604
ATTN: Propulsion Division
(SAVDL-EU-PP)

U.S. Army Artillery Combat
Developments Agency
Fort Sill, Oklahoma
ATTN: Commanding Officer

U.S. Army Missile Command
Redstone Arsenal, Alabama 35809
ATTN: AMSMI-RR

U.S. Army Missile Command
Redstone Scientific Information Center
Redstone Arsenal, Alabama 35809
ATTN: Chief, Document Section

NASA Headquarters
Aeronautical Propulsion Division
Code RL, Deputy Director
Office of Advanced Research & Technology
Washington, D.C. 20546
ATTN: Mr. Nelson F. Rekos

NASA Ames Research Center
Deputy Chief Aeronautics Division
Mail Stop 27-4
Moffett Field, California 94035
ATTN: Mr. Edward W. Perkins

NASA Langley Research Center
Hampton, Virginia 23365
ATTN: Dr. Robert S. Levine
Mail Stop 213

NASA Lewis Research Center
21000 Brookpark Road
Cleveland, Ohio 44135
ATTN: D. Morris, Mail Stop 60-3

NASA Lewis Research Center
Hypersonic Propulsion Section
Mail Stop 6-1
21000 Brookpark Road
Cleveland, Ohio 44135
ATTN: Dr. Louis A. Povinelli

NASA Marshall Space Flight Center
S&E ASTN-P
Huntsville, Alabama 35812
ATTN: Mr. Keith Chandler

National Science Foundation
Engineering Energetics
Engineering Division
Washington, D.C. 20550
ATTN: Dr. George Lee

National Science Foundation
Engineering Energetics
Engineering Division
Washington, D.C. 20550
ATTN: Dr. M. Ojalvo

National Science Foundation
Engineering Energetics
Engineering Division
Washington, D.C. 20550
ATTN: Dr. Royal Rostenbach

National Technical Information Service
Department of Commerce
5285 Port Royal Road
Springfield, Virginia 22151
ATTN: Chief, Input Section

Naval Air Development Center
Commanding Officer (AD-5)
Johnsville, Pennsylvania
ATTN: NADC Library

Naval Air Propulsion Test Center (R&T)
Trenton, New Jersey 08628
ATTN: Mr. Al Martino

Naval Air Systems Command
Department of the Navy
Washington, D.C. 20360
ATTN: Research Administrator
AIR 310

Naval Air Systems Command
Department of the Navy
Washington, D.C. 20360
ATTN: Propulsion Technology Admin
AIR 330

Naval Air Systems Command
Department of the Navy
Washington, D.C. 20360
ATTN: Technical Library Division
AIR 604

Naval Ammunition Depot
Research and Development Department
Building 190
Crane, Indiana 47522
ATTN: Mr. B. E. Douda

Naval Ordnance Laboratory Commander
White Oak
Silver Springs, Maryland 20910
ATTN: Library

Naval Ordnance Systems Command
Department of the Navy
Washington, D.C. 20360
ATTN: ORD 0331

Naval Postgraduate School
Department of Aeronautics, Code 57
Monterey, California 93940
ATTN: Dr. Allen E. Fuhs

Naval Postgraduate School
Library (Code 2124)
Monterey, California 93940
ATTN: Superintendent

Naval Postgraduate School
Monterey, California 93940
ATTN: Library (Code 0212)

Office of Naval Research Branch Office
1030 East Green Street
Pasadena, California 91106
ATTN: Dr. Rudolph J. Marcus

Office of Naval Research Branch Office
San Francisco Area
50 Fell Street
San Francisco, California 94102

Office of Naval Research Branch Office
536 S. Clark Street
Chicago, Illinois 60605
ATTN: Director

Office of Naval Research Branch Office
New York Area
207 W. 24th Street
New York, New York 10011
ATTN: Director

Office of Naval Research Branch Office
495 Summer Street
Boston, Massachusetts 02210
ATTN: Director

Office of Naval Research
Power Branch, Code 473
Department of the Navy
Arlington, Virginia 22217

Office of Naval Research
Fluid Dynamics Branch, Code 438
Department of the Navy
Washington, D.C.
ATTN: Mr. Morton Cooper

Naval Research Lab
Code 7710
Washington, D.C. 20390
ATTN: W. W. Balwanz

Naval Research Laboratory Director
Washington, D.C. 20390
ATTN: Technical Information Div.

Naval Research Laboratory Director
Washington, D.C. 20390
ATTN: Library Code 2629 (ONRL)

Naval Ship Research and Development Center
Annapolis Division
Annapolis, Maryland 21402
ATTN: Library, Code A214

Naval Ship Systems Command
Department of the Navy
Washington, D.C. 20360
ATTN: Technical Library

Naval Weapons Center Commander
China Lake, California 93555
ATTN: Airbreathing Propulsion Branch
Code 4583

Naval Weapons Center
Chemistry Division
China Lake, California 93555
ATTN: Dr. William S. McEwan
Code 605

Naval Weapons Center
Commander
China Lake, California 93555
ATTN: Technical Library

Naval Weapons Center
Code 608, Thermochemistry Group
China Lake, California 93555
ATTN: Mr. Edward W. Price, Head

Naval Weapons Laboratory
Dahlgren, Virginia 22448
ATTN: Technical Library

Naval Undersea Research and
Development Center
San Diego, California 92132
ATTN: Technical Library
Code 1311D

Naval Underwater Systems Center
Fort Trumbull
New London, Connecticut 06320
ATTN: Technical Library

Naval Underwater Systems Center
Code 5B-331
Newport, Rhode Island 02840
ATTN: Dr. Robert Lazar

Picatinny Arsenal
Commanding Officer
Dover, New Jersey 07801
ATTN: Technical Information Lib.

State Documents Section
Exchange and Gift Division
Washington, D.C. 20540
ATTN: Library of Congress

LABORATORIES AND COMPANIES

AeroChem Research Laboratories, Inc.
P.O. Box 12
Princeton, New Jersey 08540
ATTN: Dr. Arthur Fontijn

AeroChem Research Laboratories, Inc.
P.O. Box 12
Princeton, New Jersey 08540
ATTN: Library

Aerojet Liquid Rocket Company
P.O. Box 13222
Sacramento, California 95813
ATTN: Technical Information Center

Aeronautical Res. Assoc. of Princeton
50 Washington Road
Princeton, New Jersey 08540
ATTN: Dr. Guido Sandri

Aeroprojects, Inc.
West Chester
Pennsylvania 19380

The Aerospace Corporation
P.O. Box 92957
Los Angeles, California 90009
ATTN: Mr. Alexander Muraszew

Atlantic Research Corporation
5390 Cherokee Avenue
Alexandria, Virginia 22314
ATTN: Dr. Andrej Macek

Atlantic Research Corporation
5390 Cherokee Avenue
Alexandria, Virginia 22314
ATTN: Librarian

Atlantic Research Corporation
5390 Cherokee Avenue
Alexandria, Virginia 22314
ATTN: Dr. Kermit E. Woodcock
Manager, Propulsion

Avco Everett Research Laboratory
Everett, Massachusetts 02149
ATTN: Librarian

Avco Everett Research Laboratory
2385 Revere Beach Parkway
Everett, Massachusetts 02149
ATTN: Mr. Donald Leonard

Avco Lycoming Corporation
550 South Main Street
Stratford, Connecticut 06497
ATTN: Mr. John W. Schrader
Asst. Director R & D

Ballistics Research Laboratory
Commanding Officer
Aberdeen Proving Ground, Maryland
ATTN: Library

Battelle
Columbus Laboratories
505 King Avenue
Columbus, Ohio 43201
ATTN: Mr. Abbott A. Putnam
Atmospheric Chemistry &
Combustion Systems Div.

Beech Aircraft Corporation
9709 East Central
Wichita, Kansas 67201
ATTN: William M. Byrne, Jr.

Bell Aerospace Company
P.O. Box 1
Buffalo, New York 14240
ATTN: Dr. John H. Morgenthaler
C-84

Bell Aerospace Company
Advanced Technology Research
P.O. Box 1
Buffalo, New York 14240
ATTN: Dr. George Rudinger C-84

Bell Aerospace Company
P.O. Box 1
Buffalo, New York 14240
ATTN: Technical Library

Bureau of Mines
Bartlesville Energy Research Center
Box 1398
Bartlesville, Oklahoma 74003

Calspan Corporation
Aerodynamic Research Department
P.O. Box 235
Buffalo, New York 14221
ATTN: Dr. John W. Daiber

Calspan Corporation
4455 Genessee Street
Buffalo, New York 14221
ATTN: Head Librarian

Convair Aerospace Division
Manager of Propulsion
P.O. Box 748
Fort Worth, Texas 76101
ATTN: L. H. Schreiber

Detroit Diesel Allison Division
P.O. Box 894
Indianapolis, Indiana 46206
ATTN: Dr. Sanford Fleeter

Dynalysis of Princeton
20 Nassau Street
Princeton, New Jersey 08540
ATTN: Dr. H. J. Herring

Ecole Royale Militaire
30, Avenue de la Renaissance
Bruxelles B-1040, Belgium
ATTN: Prof. Emile Tits

Fairchild Industries
Fairchild Republic Division
Farmingdale, New York 11735
ATTN: Engineering Library

Flame Research, Inc.
P.O.Box 10502
Pittsburgh, Pennsylvania 15235
ATTN: Dr. John Manton

Forest Fire and Engineering Research
Pacific Southwest Forest & Range
Experiment Station
P.O. Box 245
Berkeley, California 94701
ATTN: Assistant Director

Garrett Corporation
AiResearch Manufacturing Company
Sky Harbor Airport
402 South 36th Street
Phoenix, Arizona 85034
ATTN: Mr. Aldo L. Romanin, Mgr.
Aircraft Propulsion Engine
Product Line

General Dynamics
Electro Dynamic Division
P.O. Box 2507
Pomona, California 91766
ATTN: Library MZ 6-20

General Dynamics
P.O. Box 748
Fort Worth, Texas 76101
ATTN: Technical Library
MZ 2246

General Electric Company
AEG Technical Information Center
Mail Drop N-32, Building 700
Cincinnati, Ohio 45215
ATTN: J.J. Brady

General Electric Company
Corporate Research & Development
P.O. Box 8
Schenectady, New York 12301
ATTN: Dr. Marshall Lapp

General Electric Company
GSPO-Bldg. 174AE
1000 Western Avenue
West Lynn, Massachusetts 01910
ATTN: Mr. W. Bruce Gist

General Electric Space Sciences Lab
Valley Forge Space Tech. Center
Room M-9144
P.O. Box 8555
Philadelphia, Pennsylvania 19101
ATTN: Dr. Theodore Baurer

General Motors Corporation
Detroit Diesel-Allison Division
P.O. Box 894
Indianapolis, Indiana 46206
ATTN: Mr. Millard E. Barrett, Chief Engineer, Advanced Development
Mail Stop U-27

General Motors Technical Center
Passenger Car Turgine Development
General Motors Engineering Staff
Warren, Michigan 48090
ATTN: T. F. Nagey, Director

Grumman Aerospace Corporation
Manager Space Vehicle Development
Bethpage, New York
ATTN: Mr. O. S. Williams

Mr. Daniel L. Harshman
11131 Embassy Drive
Cincinnati, Ohio 45240

Hercules Incorporated
Allegany Ballistics Laboratory
P.O. Box 210
Cumberland, Maryland 21502
ATTN: Mrs. Louise S. Derrick
Librarian

Hercules Incorporated
P.O. Box 98
Magna, Utah 84044
ATTN: Library 100-H

A/S Kongsberg Vaapenfabrikk
Gas Turbine Division
3601 Kongsberg, Norway
ATTN: R. E. Stanley
Senior Aerodynamicist

LTV Vought Aeronautics Company
Flight Technology, Project Engineer
P.O. Box 5907
Dallas, Texas 75222
ATTN: Mr. James C. Utterback

Lockheed-Georgia Company
Dept. 72-47, Zone 259
Marietta, Georgia 30060
ATTN: William A. French

Lockheed Missiles & Space Company
3251 Hanover Street
Palo Alto, California 94304
ATTN: Palo Alto Library 52-52

Lockheed Propulsion Company
Scientific and Technical Library
P.O. Box 111
Redlands, California 92373
ATTN: Head Librarian

Los Alamos Scientific Laboratory
P.O. Box 1663
Los Alamos, New Mexico 97544
ATTN: J. Arthur Freed

The Marquardt Company
CCI Aerospace Corporation
16555 Saticoy Street
Van Nuys, California 91409
ATTN: Library

Martin-Marietta Corporation
P.O. Box 179
Denver, Colorado 90201
ATTN: Research Library 6617

Martin-Marietta Corporation
Orlando Division
P.O. Box 5837
Orlando, Florida 32805
ATTN: Engineering Library, mp-30

McDonnell Aircraft Company
P.O. Box 516
St. Louis, Missouri 63166
ATTN: Research & Engineering Library
Dept. 218 - Bldg. 101

McDonnell Douglas Corporation
Project Propulsion Engineer
Dept. 243, Bldg. 66, Level 2S
P.O. Box 516
St. Louis, Missouri 63166
ATTN: Mr. William C. Paterson

McDonnell Douglas Corporation
Research Laboratories
St. Louis, Missouri 63166
ATTN: Miklos Sajben
Associate Scientist

McDonnell Douglas Astronautics Company
5301 Bolsa Avenue
Huntington Beach, California 92647
ATTN: A3-328 Technical Library

Ministry of Defense
Procunement Executive
(Room 2165) Main Building
Whitehall Gardens
London SW1, England
ATTN: Mr. L.F. Nicholson EB, idc
Vice Controller of Aircraft

National Aerospace (NLR)
Voorsterweg 31
Noord-Oost-Polder-Emmelord
Netherlands
ATTN: Mr. F. Jaarsma

National Research Council
Division of Mechanical Engineering
Montreal Road, Ottawa
Ontario, Canada KIA OR6
ATTN: Dr. R.B. Whyte

Nielsen Engineering & Research, Inc.
510 Clyde Avenue
Mountain View, California 94040
ATTN: Dr. Jack N. Nielsen

Nissan Motor Company, Ltd.
3-5-1, Momoi, Suginami-ku
Tokyo, Japan 167
ATTN: Dr. Y. Toda

Northrop Corporation
Ventura Division
1515 Rancho Conejo Boulevard
Newbury Park, California 91230
ATTN: Technical Information Center

Norwegian Defense Research Establishment
Superintendent NDRE
P. O. Box 25
2007 Kjeller, Norway
ATTN: Mr. T. Krog

ONERA
Energie and Propulsion
29 Avenue de la Division Leclure
92 Chatillon sous Bagneux, France
ATTN: Mr. M. Barrere

ONERA
Energie and Propulsion
29 Avenue de la Division Leclure
92 Chatillon sous Bagneux, France
ATTN: Mr. J. Fabri

ONERA
Energie and Propulsion
29 Avenue de la Division Leclure
92 Chatillon sous Bagneux, France
ATTN: Mr. Viaud

ONERA - DED
External Relations and
Documentation Department
29, Avenue de la Division Leclure
92320 Chatillon, France
ATTN: Mr. M. Salmon

Professor K. Papailiou
Residence les Closeaux, #21
109, Route de Morsang
91, Saintry, France

Mr. J. Richard Perrin
16261 Darcia Avenue
Encino, California 91316

Philco-Ford Corporation
Aeronutronic Division
Ford Road
Newport Beach, California 92663
ATTN: Technical Inf. Center

Pratt and Whitney Aircraft
Project Engineer, Advanced
Military System
Engineering Dept. - 2B
East Hartford, Connecticut 06108
ATTN: Mr. Donald S. Rudolph

Pratt and Whitney Aircraft Division
United Aircraft Company
400 S. Main Street
East Hartford, Connecticut 06108
ATTN: Mr. Dana B. Waring
Manager-Product Technology

Pratt and Whitney Aircraft
Program Manager, Advanced
Military Engineer
Engineering Department - 2B
East Hartford, Connecticut 06108
ATTN: Dr. Robert I. Strough

Pratt and Whitney Aircraft
Florida Research & Development Ctr.
P.O. Box 2691
West Palm Beach, Florida 33402
ATTN: Mr. William R. Alley
Chief of Applied Research

RCA Corporation
Missile and Surface Radar Division
Moorestown, New Jersey 08057
ATTN: Engineering Library
Bldg. 101-222

Rocket Research Corporation
11441 Willow Road
Redmond, Washington 98052
ATTN: Thomas A. Groudle

Rocketdyne Division
North American Rockwell
6633 Canoga Avenue
Canoga Park, California 91304
ATTN: Technical Information
Center; D/596-108

Rocketdyne Division
North American Rockwell
6633 Canoga Avenue AA67
Canoga Park, California 91304
ATTN: Mr. Henry C. Wieseneck
Manager

Rohr Corporation
Manager Advanced Technology
Engineering Division
Chula Vista, California 92012
ATTN: Mr. Joseph S. Mount

Rolls-Royce (1971) Limited
Derby Engine Division
P.O. Box 31
Derby DE2 8BJ
London, England
ATTN: C. Freeman, Installation
Research Department

Sandia Laboratories
P.O. Box 969
Livermore, California
ATTN: Dr. Dan Hartley, Div. 8351

Sandia Laboratories
Livermore, California 94550
ATTN: Robert Gallagher

Sandia Laboratories
P.O. Box 5800
Albuquerque, New Mexido 87115
ATTN: Technical Library, 3141

Solar
2200 Pacific Highway
San Diego, California 92112
ATTN: Librarian

Standard Oil Company (Indiana)
P.O. Box 400
Naperville, Illinois 60540
ATTN: R.E. Pritz

Teledyne CAE
1330 Laskey Road
Toledo, Ohio 43601
ATTN: Technical Library

TRW Systems
One Space Park
Redondo Beach, California 90278
ATTN: Mr. F.E. Fendell (R1/1004)

TRW Systems Group
One Space Park
Bldg. 0-1 Room 2080
Redondo Beach, California 90278
ATTN: Mr. Donald H. Lee, Manager

Ultrasystems, Inc.
500 Newport Center Drive
Newport Beach, California 92660
ATTN: Dr. David C. Wooten
Research Scientist

United Aircraft Research Laboratory
East Hartford, Connecticut 06108
ATTN: Dr. Frank Carta

United Aircraft Research Laboratory
East Hartford, Connecticut 06108
ATTN: Librarian

Valley Forge Space Tech. Center
P.O. Box 8555
Philadelphia, Pennsylvania 19101
ATTN: Dr. Bert Zauderer

Vought Missiles & Space Company
P.O. Box 6267
Dallas, Texas 75222
ATTN: Library - 3-41000

Xonics
6849 Hayvenhurst Avenue
Van Nuys, California 91406
ATTN: Dr. Vincent LoDato
Principal Research Scientist

UNIVERSITIES AND INSTITUTES

Boston College
Department of Chemistry
Chestnut Hill, Massachusetts 02167
ATTN: Rev. Donald MacLean, S.J.
Associate Professor

Polytechnic Institute of Brooklyn
Department of Aerospace Engineering
and Applied Mechanics
Farmingdale, New York 11735
ATTN: Dr. Samual Lederman

Brown University
Division of Engineering
Box D
Providence, Rhode Island 02912
ATTN: Dr. R. A. Dobbins

California Institute of Technology
Department of Chemical Engineering
Pasadena, California 91109
ATTN: Prof. W. H. Corcoran

California Institute of Technology
Jet Propulsion Laboratory
4800 Oak Grove Drive
Pasadena, California 91103
ATTN: Library

California Institute of Technology
Div. of Engineering & Applied Science
Pasadena, California 91109
ATTN: Prof. Anatol Roshko

University of California, San Diego
Dept. of Aerospace and Mechanical
Engineering
La Jolla, California 92037
ATTN: Professor Paul Libby

University of California, San Diego
Dept. of Engineering Physics
P.O. Box 109
La Jolla, California 92037
ATTN: Professor S. S. Penner

University of California
School of Engineering and Applied
Science
7513 Boelter Hall
Los Angeles, California 90024
ATTN: Engineering Reports Group

University of California
Lawrence Radiation Laboratory
P.O. Box 808
Livermore, California 94550
ATTN: Technical Information Dept.
L-3

University of California
General Library
Berkeley, California 94720
ATTN: Documents Department

Case Western Reserve University
School of Engineering
Div. of Fluid, Thermal and
Aerospace Sciences
Cleveland, Ohio 44106
ATTN: Professor J. S. T'ien

Case Western Reserve University
10900 Euclid Avenue
Cleveland, Ohio 44106
ATTN: Sears Library - Reports
Department

Case Western Reserve University
Division of Fluid Thermal and
Aerospace Sciences
Cleveland, Ohio 44106
ATTN: Professor Eli Reshotko

Colorado State University
Engineering Research Center
Fort Collins, Colorado 80521
ATTN: Mr. V. A. Sandborn

The University of Connecticut
Department of Mechanical Engineering
U-139
Storrs, Connecticut 06268
ATTN: Professor E. K. Dabora

Cooper Union
School of Engineering and Science
Cooper Square
New York, New York
ATTN: Dr. Wallace Chintz
Associate Professor of ME

Cornell University
Department of Chemistry
Ithaca, New York 14850
ATTN: Professor Simon H. Bauer

Technical University of Denmark
Fluid Mechanics Department
Building 404 2800 Lyngby
DK-Denmark
ATTN: Professor K. Refslund

Franklin Institute Research Laboratories
Philadelphia, Pennsylvania 19103
ATTN: Dr. G. P. Wachtell

Fysisch Laboratorium
Fijksuniversiteit Utrecht
Sorbonnelaan
Utrecht, The Netherlands
ATTN: Dr. F. van der Valk

Georgia Institute of Technology
Atlanta, Georgia 30332
ATTN: Price Gilbert Memorial
Library

Georgia Institute of Technology
School of Aerospace Engineering
Atlanta, Georgia 30332
ATTN: Dr. Ben T. Zinn
Professor

University of Illinois
Department of Energy Engineering
Box 4348
Chicago, Illinois 60680
ATTN: Professor Paul M. Chung

University of Illinois
College of Engineering
Dept. of Energy Engineering
Chicago, Illinois
ATTN: Dr. D. S. Hacker

Imperial College
London, England
ATTN: Professor Gaydon

Imperial College of Science
and Technology
Department of Mechanical Engineering
Exhibition Road
London, S.W.7, England
ATTN: Professor W. Murgatroyd

The Johns Hopkins University
Applied Physics Laboratory
8621 Georgia Avenue
Silver Spring, Maryland 20910
ATTN: Chemical Propulsion
Information Agency

The Johns Hopkins University
Applied Physics Laboratory
8621 Georgia Avenue
Silver Spring, Maryland
ATTN: Document Librarian

The Johns Hopkins University
Applied Physics Laboratory
8621 Georgia Avenue
Silver Spring, Maryland
ATTN: Dr. A. A. Westenberg

University of Leeds
Leeds, England
ATTN: Professor Dixon-Lewis

Massachusetts Institute of Technology
Dept. of Chemical Engineering
Cambridge, Massachusetts 02139
ATTN: Dr. Jack B. Howard

Massachusetts Institute of Technology
Department of Chemistry, Room 6-123
Cambridge, Massachusetts 02139
ATTN: Dr. John Ross

MIT Libraries Room 14 E-210
77 Massachusetts Avenue
Cambridge, Massachusetts 02139
ATTN: Technical Reports

Massachusetts Institute of Technology
Room 10-40[illegible]
Cambridge, Massachusetts 02139
ATTN: Engineering Technical Reports

Massachusetts Institute of Technology
Dept. of Mechanical Engineering
Room 3-246
Cambridge, Massachusetts 02139
ATTN: Professor James Fay

Massachusetts Institute of Technology
Dept. of Mechanical Engineering
Cambridge, Massachusetts 02139
ATTN: Professor Robert Stickney

University of Michigan
Dept. of Aerospace Engineering
Ann Arbor, Michigan 48105
ATTN: Prof. T. C. Adamson, Jr.

Midwest Research Institute
425 Volker Boulevard
Kansas City, Missouri 64100
ATTN: Dr. T. A. Milne

Mitglied des Vorstands der Fried.
Krumpp GmbH
43 Essen, AltendorferstraBe 103
Germany
ATTN: Wilhelm Dettmering
Professor Dr.-Ing.

New York Institute of Technology
Wheatley Road
Old Westbury, New York 11568
ATTN: Dr. Fox

University of North Carolina
Periodicals and Serials Division
Drawer 870 Library
Chapel Hill, North Carolina 27514
ATTN: Mr. Stephen Berk

University of Notre Dame
Serials Record
Memorial Library
Notre Dame, Indiana 46556
ATTN: B. McIntosh

University of Notre Dame
College of Engineering
Notre Dame, Indiana 46556
ATTN: Stuart T. McComas,
Assistant Dean for Research
and Special Projects

Ohio State University
Dept. of Chemical Engineering
140 West 19th Avenue
Columbus, Ohio
ATTN: Dr. Robert S. Brodkey

Orta Dogu Teknik Universitesi
Mechanical Engineering Department
Ankara, Turkey
ATTN: Professor H. Sezgen

The Pennsylvania State University
Room 207 Old Main Building
University Park, Pennsylvania 16802
ATTN: Office of Vice President
for Research

Pennsylvania State University
College of Engineering
University Park, Pennsylvania 16802
ATTN: Dr. Otis E. Lancaster
Engineering Education

Pennsylvania State University
Ordnance Research Laboratory
University Park, Pennsylvania 16802
ATTN: Mr. Edgar P. Bruce

Institute Politechnico Nacional
Unidad Profesional de Zecatenco
Mexico 14, D. F. Mexico
ATTN: Ing. Manuel Zorrilla
Director General

Princeton University
Dept. of Aerospace and Mech. Sciences
James Forrestal Campus
Princeton, New Jersey 08540
ATTN: Dr. Martin Summerfield

Princeton University
Forrestal Campus Library
P.O. Box 710
Princeton, New Jersey 08540
ATTN: V. N. Simosko, Librarian

Purdue University
Aeronautics, Astronautics, and
Engineering Sciences
Grissom Hall
West Lafayette, Indiana 47907
ATTN: Library

Purdue University
School of Mechanical Engineering
West Lafayette, Indiana 47907
ATTN: Prof. V. W. Goldschmidt

Purdue University
School of Mechanical Engineering
West Lafayette, Indiana 47907
ATTN: Professor S.L.K. Wittig

Purdue University Advisors

D.E. Abbott	TSPC
W.F. Edgell	CHEM
R. Goulard	TSPC
M.R. L'Ecuyer	TSPC
F.J. Marshall	AAES
A.M. Mellor	TSPC
S.N.B. Murthy	TSPC
J.R. Osborn	TSPC
J.G. Skifstad	TSPC
B.A. Reese	TSPC

Queen Mary College
Dept. of Mechanical Engineering
Thile Eld Road
London El, England
ATTN: Professor M. W. Thring

Rice University
Welch Professor of Chemistry
Houston, Texas 77001
ATTN: Dr. Joseph L. Franklin

University of Rochester
Dept. of Chemical Engineering
Rochester, New York 14627
ATTN: Dr. John R. Ferron

Rome University
Via Bradano 28
00199 Rome, Italy
ATTN: Prof. Gaetano Salvatore

Sener
Departamento de Investigation
Km. 22.500 de la antigua carretera
Madrid - Barcelona
Spain
ATTN: Mr. J. T. Diez Roche

Sophia University
Science and Engineering Faculty
Kioi 7
Tokyo-Chiyoda, Japan 102
ATTN: Professor M. Suzuki

Southern Methodist University
Thermal and Fluid Sciences Center
Institute of Technology
Dallas, Texas 75275
ATTN: Prof. Roger L. Simpson

Stanford Research Institute
Department of Chemical Dynamics
Menlo Park, California 94025
ATTN: Dr. Henry Wise

Stanford University
Department of Aeronautics and
Astronautics
Stanford, California 94305
ATTN: Dr. Walter G. Vincenti

Stanford University
Dept. of Mechanical Engineering
Stanford, California 94305
ATTN: Professor A. L. London

Stevens Research Institute
Castle Point Station
Hoboken, New Jersey 07030
ATTN: Prof. Robert F. McAlevy III
Combustion Lab Director

Stevens Institute of Technology
Department of Mechanical Engineering
Castle Point Station
Hoboken, New Jersey 07030
ATTN: Professor Fred Sisto

University of Tokyo
Department of Reaction Chemistry
Faculty of Engineering
Bunkyo-ku
Tokyo, Japan 113
ATTN: Professor T. Hikita

University of Virginia
Dept. of Aerospace Engineering
School of Engineering and
Applied Science
Charlottesville, Virginia 22901
ATTN: Dr. John E. Scott

University of Virginia
Science/Technology Information Ctr.
Charlottesville, Virginia 22901
ATTN: Richard H. Austin

Virginia Polytechnic Institute and
State University
Dept. of Aerospace Engineering
Blacksburg, Virginia 24061
ATTN: Dr. George R. Inger

Virginia Polytechnic Institute and
State University
Mechanical Engineering Department
Blacksburg, Virginia 24061
ATTN: Mr. Walter F. O'Brien, Jr.

George Washington University Library
Washington, D.C. 20006
ATTN: Reports Section

Yale University
Engineering and Applied Science
Mason Laboratory
New Haven, Connecticut 06520
ATTN: Dr. John B. Fenn

Yale University
Mason Laboratory
400 Temple Street
New Haven, Connecticut 06520
ATTN: Prof. Peter P. Wegener

SECURITY CLASSIFICATION OF THIS PAGE *(When Data Entered)*

REPORT DOCUMENTATION PAGE

READ INSTRUCTIONS BEFORE COMPLETING FORM

1. REPORT NUMBER: CIT-7-PU	2. GOVT ACCESSION NO.
3. RECIPIENT'S CATALOG NUMBER	
4. TITLE *(and Subtitle)*: Large Structure Dynamics and Entrainment in the mixing layer at High Reynolds number.	5. TYPE OF REPORT & PERIOD COVERED: Technical Report 1975
	6. PERFORMING ORG. REPORT NUMBER
7. AUTHOR(s): Paul E. Eimotakis and Garry L. Brown	8. CONTRACT OR GRANT NUMBER(s): N00014-75-C-1143 NR-098038
9. PERFORMING ORGANIZATION NAME AND ADDRESS: Graduate Aeronautical Laboratories California Institute of Technology Pasadena, California	10. PROGRAM ELEMENT, PROJECT, TASK AREA & WORK UNIT NUMBERS
11. CONTROLLING OFFICE NAME AND ADDRESS: Project SQUID, Thermal Sciences and Propulsion Center, Purdue University, West Lafayette, Indiana 47907	12. REPORT DATE: October 1975
	13. NUMBER OF PAGES: 56
14. MONITORING AGENCY NAME & ADDRESS *(if different from Controlling Office)*: Office of Naval Research, Power Program Code 473, Department of the Navy Arlington, VA 22217	15. SECURITY CLASS. *(of this report)*: Unclassified
	15a. DECLASSIFICATION/DOWNGRADING SCHEDULE
16. DISTRIBUTION STATEMENT *(of this Report)*	
17. DISTRIBUTION STATEMENT *(of the abstract entered in Block 20, if different from Report)*	
18. SUPPLEMENTARY NOTES	
19. KEY WORDS *(Continue on reverse side if necessary and identify by block number)*: Turbulence structure, Reynolds number effect Entrainment Mixing	

20. ABSTRACT *(Continue on reverse side if necessary and identify by block number)*

Observations were made on a turbulent mixing layer in a water channel at Reynolds numbers up to 3×10^6. Flow visualization with dyes revealed (once more) large coherent structures and showed their role in the intrainment process; observations of the reaction of a base and an acid indicator injected on the two sides of the layer, respectively, gave some indication of where molecular mixing occurs. Autocorrelations of streamwise velocity

(cont.)

DD FORM 1 JAN 73 1473 EDITION OF 1 NOV 65 IS OBSOLETE S/N 0102-014-6601 |

UNCLASSIFIED

SECURITY CLASSIFICATION OF THIS PAGE *(When Data Entered)*

CONT.

fluctuations, using an LDV, revealed a fundamental periodicity associated with the large structures. The surprisingly long correlation times suggest time scales much longer than had been supposed; it is argued that the mixing layer dynamics at any point is coupled to the large structure further downstream, and some possible consequences about the effects of initial conditions and of the influence of apparatus geometry are discussed.